OPTIMAL MARINE FARM STRUCTURES

A thesis submitted in partial fulfilment
of the requirements for the
Degree of Doctor of Philosophy
in Computational and Applied Mathematics
by Alistair Smith

UNIVERSITY OF CANTERBURY

2003

ACKNOWLEDGEMENTS

This research was funded by the National Institute of Water and Atmospheric Research (NIWA) New Zealand and by the New Zealand Foundation for Research Science & Technology (FRST), Enterprise Scholarship contract CO1X0003.

I would like to thank my supervisors, Dr Vladimir Nikora, Dr Alex Ross and Prof. Graeme Wake, for their support and direction. In particular, Vladimir's passion for science, Alex's broad perspective, Graeme's consistent encouragement, as well as their individual expertise and supervisory teamwork, have enabled the completion of this thesis.

Lastly, I could not have made it through the last three years without the continued support from my amazing wife, Amanda, and from my officemate, and good friend, Rob Ware.

ABSTRACT

This thesis documents a new modelling approach for assessing the interplay between marine mussels and their environment, and presents the development of multi-scale methodology for addressing the question of optimal aquaculture structures. The Lattice Boltzmann (LB) method can accommodate the complex geometry of mussel clusters. This hydrodynamic model is expanded to incorporate physiological activity, in order to quantify the relationship between mussels, the surrounding flow and the spatial distribution of phytoplankton concentration (the mussel food supply). Uptake results, from simulations at the smallest scale of modelling, quantify the non-linear effect of competition for phytoplankton and are shown to be generally independent of diffusive conditions. Statistics of phytoplankton uptake and the hydrodynamic drag force of the cluster are absorbed into a second scale of consideration. Approaches for generating optimal arrangements under various physical constraints at this (medium) scale are presented and compared, following the objective of maximising collective phytoplankton uptake. It is found that branching structures are optimal in limited domains of unidirectional flow, nets perpendicular to unidirectional flow are more efficient in larger areas and spirals are optimal in flow of varied direction. Lastly, analysis of the efficiency of some presently used structures is given, along with methodological suggestions for integrating the optimisation process into large scales, such as an aqua farm in a bay environment.

CONTENTS

Chapter 1 - INTRODUCTION

The interaction between non-mobile aquatic organisms (e.g., mussels) and flow has become an increasingly important aspect of ecological studies of benthic communities. The flux of phytoplankton to suspension filter feeders and the supply of nutrients to aquatic plants are key issues affecting the productivity and composition of these communities (e.g., Frechette et al 1999, Hurd et al 1996). These fluxes are heavily influenced by the interaction of the organisms and the flow (Nikora et al 2002a, Nikora et al 2002b). Additionally, the aquaculture structures modify the forces exerted, both on themselves and on neighbouring ecosystems.

These issues are especially relevant in relation to the intensive cultivation of bivalve molluscs (e.g., Pilditch et al 2001). Bivalves are suspension filter feeders which feed by pumping water through their inhalant siphon and over their gills where particles, including phytoplankton, are extracted from the water. Shellfish are usually suspended in some way from a surface structure. They are typically attached to rope in the cases of mussels, or other such suspension systems, as in the case of scallops or oysters.

How these shellfish interact with the hydrodynamics is determined by both the environment, e.g. the abundance of plankton, and the organism arrangement (e.g., Russel-Hunter 1970, Valiela 1995). An important consequence of these interactions is flow modification, which may further complicate interactions (e.g., Grant and Bacher 2001).

The organism-flow interactions cover a wide range of scales, which can vary from the scale of the individual shellfish, to the scale of large farms, which could be several hundred hectares. Important environmental and ecological effects include the utilisation of phytoplankton in relation to neighbouring individuals of the same or other species, through to the potential for large-scale zones of phytoplankton depletion, surrounding the farm. There is also the potential for large farms to modify bay-scale hydrodynamics,

which in turn may have significant feedback on the farm itself. Ultimately these interactions will give rise to modifications in the growth and condition of the shellfish and their environment. Hence there is a need to incorporate these effects into dynamic models of shellfish energetics (e.g., Ross and Nisbet 1991, Ren and Ross 2001) and the ecosystem (e.g., Ross et al 1994) for determining system carrying capacity. One of the key problems in such a task is producing a realistic representation of how the farm structures modify, and are affected by, the flow.

Coupled with the assessment of ecosystem carrying capacity is the need to quantify the efficiency of existing farms and the identification of optimal structures for potential future farms. Such optimality would pertain to the full range of hydrodynamic scales. The task of finding optimal structures would therefore require, not only modelling of the multi-scale interplay between structure and environment, but a sound methodological framework to support and complement theoretical results.

This thesis addresses the dynamics between mussels and their environment, in the pursuit of mussel farm structure optimality. The main objective is to identify the arrangement of mussels (*Perna canaliculus*) that will maximise the collective efficiency, defined in terms of phytoplankton uptake statistics.

Considerations on general methodology are presented in Chapter 2, first by defining terms, then giving possible criteria sets for optimality and identifying logistic constraints. With this perspective on optimisation, the physical domain will be addressed, in terms of how a large environment such as a bay might be subdivided into a hierarchical organisation of scales of simulation. The role and treatment of independent variables for each scale will then be considered, as well as the numerical values for constants.

Chapter 3 first outlines the motivation for the Lattice Boltzmann (LB) method to model the hydrodynamics, then discusses relevant theory, model implementation, coding issues and testing. A specific model is subsequently developed, incorporating biophysical aspects of the system, such as plankton dynamics, mussel geometry and filtration.

The grid resolution for the first and smallest scale of modelling is 0.004 m. Documentation of simulations at this scale is presented in Chapter 4, including the issues surrounding the arrangement of mussels on a rope, the sensitivity of uptake efficiency to phytoplankton diffusivity, variation of the rope's orientation to the flow and the drag force on the structure. Numerical results are given, along with discussion, also analysis of the uptake distribution for the optimal configuration.

The second (i.e., medium) scale of simulation, presented in Chapter 5, widens the scope to address variation in flow properties and models at a grid resolution of 0.22 m. Various models and techniques for generation of optimal arrangements are outlined, their results are compared and discussed.

Chapter 6, on large scale simulation, gives an assessment of the efficiency of current structures. It also provides a theoretical framework for optimality at the bay scale, which involves some multi-scale methodology.

A summary of work done, significant results and their practical application, is given in Chapter 7, along with discussion of modelling assumptions and possibilities for future work in this area.

Chapter 2 - METHODOLOGY

Methodological issues will be addressed here, which are vital in simulations of complex systems. These issues are especially sensitive given the spatial and temporal scales of consideration that span several orders of magnitude, from an individual mussel to an entire bay.

This Chapter will begin with discussion and definitions relating to the measure of efficiency of a given arrangement, in order to facilitate structure optimisation.

2.1 Optimality Criteria

Optimality problems consist of an objective function, usually combined with one or more constraints. Quantifying the objective function in the case of farm performance is difficult, since it requires speculation on the individual needs and economic perspectives of mussel farmers. It is possible, however, to identify certain properties of farms that would imply general efficiency. These properties form a pool of possible criteria, from which a quantitative objective function can be formulated that will provide explicit definitions of optimality for generic application.

Properties indicative of efficiency of a group of mussels will depend on the assessment of efficiency of a single mussel. Hence, some measure that usefully expresses a mussel's uptake rate must first be defined. From the perspective of optimality, actual values are not relevant, simulations will compute relative quantities of uptake only. The justification for this is that the true functional response of the mussel (e.g., Valiela 1995) is in relation to total particulate concentrations, which are much greater (in terms of both volume and weight) than phytoplankton concentrations. Total particulate concentrations in mussel culture situations are typically well below the measured half-saturation functional

response and therefore the response is justifiably linear in relation to increasing phytoplankton concentration (Figure 1).

For numerical convenience, a nominal ambient phytoplankton concentration of 1 is assumed, as is a potential maximal uptake rate of 1. This maximum would be attained in the hypothetical scenario of a mussel on its own, in plankton-filled flow, oriented optimally, with inhalant siphon upstream. The uptake rate variable, u, will therefore take on values in the range (0,1), a low number signifying the effects of plankton depletion due to upstream mussels or disadvantageous orientation, or both.

In consideration of an ensemble of N mussels, the collective uptake can be expressed in the form of a probability density function $f(u)$. An initial possibility for the objective function here is the *sum* of the individual uptake rates u, which is directly related to total growth, or mass, of the mussel assemblage. Alternatively, the *mean* or *median* of the individual uptake rates may have more relevance for a farmer desiring higher uptake for fewer mussels. It is also important to consider the *variance* of the individual uptake rates, since it may be important for a large proportion of mussels to be within a small size range.

More practically, the concept of mussel quality is vital here, since only mussels of sufficient quality may be of commercial interest. Quality is most easily defined by a binary measure. That is, let a mussel be of good quality if and only if it uptakes plankton at a rate higher than, or equal to, some critical value u_0. If Q is defined as the number of good quality mussels, the wider optimisation task reduces to maximising Q.

The value Q is implicitly related to the sum, mean, median and variance of uptake rates, via the distribution f. Without knowing the specific form of f, this relationship cannot be formally expressed. For example, f cannot be Gaussian (Normal), since u is bounded by 0 and 1. However, some general inequalities are derivable, which translate to useful bounds on the mean, μ, the median, u_m, and the variance, σ^2.

For a given Q, the least possible values for the mean, μ, and median, u_m, result when

$u = 0$ for $N - Q$ mussels and

$u = u_0$ for Q mussels,

which lead to the inequalities

$$\mu \geq u_0 Q / N \tag{1}$$

and

$$u_m \geq u_0 \quad \text{if} \quad Q / N \geq 0.5 . \tag{2}$$

Similarly, an upper bound for the variance, σ^2, corresponds to

$u = 0$ for $N - Q$ mussels and

$u = 1$ for Q mussels,

giving

$$\sigma^2 \leq (Q / N)(1 - Q / N) . \tag{3}$$

It is also noted that the sum of uptake rates is linearly dependent on the mean, related by the total number of mussels N, so that the sum must be greater than or equal to $u_0 Q$.

These bounds indicate that the mean, median and sum of uptake rates will in general increase with increased Q, provided $Q / N > 0.5$. It is also seen that, subject to the same condition on Q / N, the variance of uptake rates will in general decrease. The objective of maximising Q (the number of good quality mussels) therefore addresses sum, mean, median and variance satisfactorily, so fulfils all requirements.

Designation of the critical uptake rate is somewhat arbitrary at this point, as it depends on many factors beyond control or consideration. For instance, the specific relationship

between uptake rate and growth of the mussel is not known, nor are the economic issues surrounding the worth and quality of mussels. However, it appears necessary to maintain $Q/N > 0.5$, due to its implications for the median and variance behaviour, as seen in the previous analysis. This requirement would lead to the imposition of a low value for u_0, since Q is a decreasing function of u_0. In contrast, the higher the u_0 value, the better the quality of mussels, so that a value too low would be unhelpful in regards to optimality. As a compromise, a value of 0.8 has been chosen, to be kept for the remainder of this thesis, unless it proves unrealistic or otherwise unsuitable.

The issue of optimality constraints includes two aspects, both arising largely from practicality. Firstly, a spatial limit will be imposed on structures, at least at the first scale of modelling. Secondly, it would generally be preferred that structures be connected somehow.

These considerations of efficiency, quality and constraint, lead to various possibilities of optimality criteria.

Criteria A

Let S be the structure, or configuration, of the set of N mussels. Let L be the domain size, that is, the length of a side of the smallest cube that encompasses S. The number of good quality mussels present, Q, is expressed as $Q = Q(N, S)$.

Thus, the first set of criteria is defined by the following:

1. S is connected.
2. L is fixed.
3. N is fixed.
4. S_o is optimal if $Q(S_o) = \max_S(Q(S))$

This is the most applicable definition of optimality. Under Criteria A, optimal shapes can be found for various N. Here N is a parameter, rather than a variable to be included in the optimisation process.

Criteria B

For the second set of criteria, the third criterion, that N must be fixed, is removed. The inclusion of N as an independent variable decreases the chances of arriving at non-trivial solutions. For instance, a maximal Q value could be attained in a given volume by completely filling that volume with mussels. An additional parameter, p, is therefore introduced, which will, like u_0, impose a quality constraint. The value for p will be between 0 and 1, representing a critical *proportion* of mussels. Specifically, this criterion imposes the requirement that the number of good quality mussels is at least a certain proportion of the total, that is,

$$Q \geq pN . \tag{4}$$

Based on the preference that $Q/N > 0.5$, it follows that p should be selected to exceed 0.5, in order to guarantee this inequality. Solutions will therefore be sought for p values in the approximate range 0.5 to 0.9.

Thus, the criteria are:

1. S is connected.
2. L is fixed.
3. (N_o,S_o) is optimal if $Q(N_o,S_o) = \max_{N,S}(Q(N,S))$ subject to $Q \geq pN$.

Criteria C

Finally, there will be some cases where there exist non-trivial structures which are optimal in the absolute sense. For identification of these structures, a set of criteria for absolute optimality is included. Set C of criteria are as follows:

1. S is connected.
2. L is fixed.
3. (N_o,S_o) is optimal if $Q(N_o,S_o) = \max_{N,S}(Q(N,S))$

It is important to note that, according to all these criteria, there may be many N_o and S_o pairs that lead to the maximum possible Q. Uniqueness of solutions is not considered to be relevant at this point, so that additional or multiple solutions are treated as inconsequential. However, this decision may be reassessed, as dictated by results.

It is foreseen that individual uptake rates will, in general, decrease with the number of mussels, N, that are present. For arrangements involving small N, a vast majority of the individual uptake rates may exceed u_0. In these scenarios, Q will not be useful as an objective function for efficiency, since it will not satisfactorily differentiate between potential configurations that produce a trivially high value for Q, for instance, $Q = N$. In these cases, other measures of efficiency will be considered, such as the mean or sum of individual uptake rates.

2.2 Scales of Modelling

The modelling of aquaculture structures covers a wide range of scales, encompassing several orders of magnitude. In theory, there is no difficulty inherent in covering such a range of scales. There is no fundamental reason why turbulent hydrodynamics and phytoplankton uptake could not be included in a model extending over an entire

aquaculture farm or bay. However, current computational limitations prevent this modelling approach; a compromise is sought between computability and complexity. The overall domain is therefore segregated into a hierarchy of specific scales, so that the processes associated with each specific scale can be maintained by modelling them separately.

Optimality considerations are also specific to each scale, in addition to applying to the multi-scale framework as a whole. It is therefore necessary to examine not only the specifics of each scale of consideration, but also the connections and relationships between them, in terms of both modelling and optimality. The general approach here is to use results from one scale, as far as they relate to structure optimality, as the input data, or parameters, for modelling at the next specific scale. Such an approach begins with the identification of potential spatial scales.

The smallest physical scale in the system is an individual mussel. This scale is therefore a possibility for the first scale of modelling. The three-dimensional geometry of one mussel would be accurately specified and physiology at this scale could be represented to the extent that it affects spatial phytoplankton distribution. Hydrodynamics would be simulated around the individual mussel in isolation.

There are three possibilities for the usefulness of modelling at that scale. The first is where all mussels are sufficiently isolated to be hydrodynamically independent. This is physically unreasonable, especially in the light of the complex mussel clusters which occur naturally.

The second possibility assumes that the hydrodynamics between mussels is dependent in a way that could be simulated numerically. This would require additional simulation and analysis to determine the effect one mussel has on another, also some numerical or algebraic approximation of the relationship between geometry, scale and plankton depletion. Further, including more than one mussel into consideration would, by definition, effectively introduce an additional scale of simulation.

Within the third possibility, a mussel could be scaled to almost fill the grid, so that in the next scale, two adjacent units would represent two adjacent mussels. This would limit the amount of potentially occurring hydrodynamics around a given mussel, also increasing the boundary effects.

Because of these problems for the single mussel scale, this scale is rejected, in favour of direct simulations of multiple mussels on a rope section. The resolution necessary to represent the complexities associated with an individual mussel must be maintained, while the model facilitates the inclusion and positioning of multiple mussels attached to a rope. Relevant physiological aspects will also be represented, such as plankton concentration and filtration by individuals.

The domain length, L, of this smallest scale will be based on the naturally occurring mussel clusters. This space is sufficiently small to allow simplifications relating to the surrounding hydrodynamics. The velocity on the domain boundary is assumed to be uniform at this scale. Further, simulations in small domains operate on a small time scale, which supports the assumption of the persistence of *direction* of the uniform flow on the domain boundary. These spatial and temporal uniformities will be considered as defining characteristics of this scale of modelling, in addition to constancy of ambient phytoplankton concentration.

The second scale of modelling will necessarily encompass a wider space and time and must therefore accommodate variation in velocity. In particular, the direction of flow may vary in time considerably in realistic settings, so must be equivalently varied in the model. The assumption that flow is spatially uniform across the domain, at any given instant, will be continued. However, the direction of this uniform flow may vary in time. As in the first scale, the concentration of phytoplankton on the boundary will be assumed to be constant.

Transition can then be made from the first scale to this with the assumption that hydrodynamic and plankton effects can be simulated at a larger scale more easily. Model resolution will be sufficiently larger than small scale turbulent effects and plankton depletion can be handled as a cumulative effect of many mussels in a cluster.

In simulations at the first scale, it is required that a statistical analysis of the depletion with various placements and orientations of individual mussels be carried out, in order to quantify the ensemble effect for this larger scale. Turbulent effects and plankton depletion can then be entered as macro-parameters from the multiple-mussel scenario. The domain of this medium scale will potentially contain multiple rope sections, providing the framework for significant contribution towards structure optimality. Consideration of uniform flow whose direction varies in time will be introduced at this scale of modelling.

Assumptions of instantaneously uniform flow and constant phytoplankton concentration are obviously unjustifiable in large scales such as a bay. Circulatory flow patterns will inevitably exist and the natural ecology of plankton will be so complex that concentration levels will be patchy at best. Progress into this scale will depend on results from the first two scales and will require the input of additional boundary conditions, such as tidal and flow data and plankton distribution. Methodology for simulation at this scale will be outlined in Chapter 6.

As a summary of this methodological discussion, modelling will involve an explicitly defined nested system of three scales. 'Small Scale' incorporates multiple mussels on a rope section, where water flow is constant in time and space and ambient plankton concentration is constant. 'Medium Scale', which extends to multiple rope sections, extends the possible conditions from the first scale by allowing temporal variation of the direction of flow. Lastly, 'Large Scale' simulates dynamics around an entire farm at the bay level, allowing spatial variation of flow direction and plankton concentration. Simulations at these three scales are documented in Chapters 4 to 6 respectively.

2.3 Variables

In order to ascertain optimal structures, arrangement must be the predominant independent variable at each scale of consideration. However, the optimal arrangement will be dependent on natural conditions such as flow variation and water diffusivity. These are therefore included as independent variables.

The form that variables will take will depend on the scale of consideration. For instance, varying the configuration at the small scale involves positioning individual mussels on a rope and altering the vertical orientation of the rope to the flow. This level of variation becomes unviable at larger scales where the number of possible configurations increases exponentially. It is possible, however, to utilise the multi-scale nature of the model, by using only the arrangement that is optimal at the small scale, in simulations at the medium scale. These optimal structures then exist as units, whose location is manipulated among several other identical units. This optimisation strategy is similarly applied in the transition from medium scale to large. The optimal arrangement at the medium scale will be assumed at the large scale, where this arrangement, in turn, becomes a unit.

How the arrangement is varied at each scale will depend on limitations of the model and on any previous indicators of what might lead to optimality. Candidates for optimal structures will come from a variety of sources, some reasoned, some intuitive. Progression will primarily be results orientated, so that the structures that yield high efficiencies will be retained regardless of their origin.

Beginning at the medium scale, velocity distribution will be varied. As mentioned, this will take the form of variation in direction of flow, as the most descriptive property of flow condition. If θ is defined as the horizontal angle of the flow, the distribution of flow direction can be described by the probability density function $g(\theta)$. A consequence of varying direction only is that the magnitude of the velocity (i.e., speed) is kept constant at a typical and arbitrary value of 0.05 m/s.

The coefficient for turbulent diffusion, D, varies with scale. Estimations for this coefficient (see Monin and Yaglom 1975, Stacey et al 2000, Stevens 2003) lead to a D value of the order 10^{-5} m^2/s at the smallest scale. However, there are many factors and physical processes that contribute to effective diffusion, depending on the environment. The value of D should make allowance for these effects. Secondly, the sensitivity of the model to diffusion is not known, in regards to which arrangements are optimal. Due to the unknown nature of D, simulations will be performed at various values, namely 0, 10^{-5}, 10^{-4} and 10^{-3} m^2/s at the small scale of modelling. This will provide sufficient scope to expose any significant sensitivity of optimal structure to the diffusion coefficient. Results here will determine subsequent methodology. In particular, in the absence of problematic sensitivity to D, a nominal typical value for the diffusion coefficient will be imposed for simulation at the medium and large scales.

The main dependent variables to be recorded are uptake rates for each mussel. The drag force will also be calculated when modelling at the smallest scale. This is so that, although the actual geometry of the clusters will not be visible in the medium and large scales, the mussels will still have a hydrodynamic effect on the water flow. The measured force can be imposed at higher scales by reducing local fluid momentum, in each unit, directly.

Physical constants relevant to simulations are the water speed, viscosity and density. As mentioned, the water speed will be kept at 0.05 m/s. It is assumed that uptake results, in particular the identification of optimal arrangements, will not be significantly sensitive to the specific values of viscosity and density. This removes the need for strict accuracy or variation in these quantities. The viscosity of water will be set to 10^{-6} m^2/s and its density to 1000 kg/m^3.

Chapter 3 - MODEL

The scientific method routinely encounters difficulties, a common example being the generation of predictions from complex hypotheses. This is the primary motivation for modelling. Models are abstract systems, calibrated with observed data, which carry vast predictive potential. Their value lies in appeal to analogy. That is, if a model resembles the physical world in some area, it is intuitive to reason that the similarity may not be confined to that area, so that new insights into the system being modelled may be obtained.

If the key to a model is the strength of the analogy on which it is built, this introduces a significant degree of subjectivity. There is no generic algorithm for constructing something which is, by definition, at least one level of abstraction separated from the universe it is designed to mimic. Instead, the conception of a model relies on incorporation of established ideas, held together by intuitive assumptions and inferences, known as auxiliary hypotheses (e.g., Lehman et al.1975).

3.1 Motivation

The main difficulties to be overcome by a potential model for current objectives, particularly at the first (small) scale of modelling, are accommodating the geometrical complexity of mussel arrangements and simulating the complicated turbulent flows that result. That these aspects are combined with physiological processes, which are not well quantified, increases the task. The fundamental auxiliary hypothesis is the assumption that the hydrodynamic processes are independent of fluctuations in plankton concentration. First, a fluid model, that can model flow around mussels, is developed. Plankton dynamics are then incorporated as a separate phase of modelling, superimposed on the first.

The geometry of a mussel cluster is problematic for traditional fluid modelling approaches based on partial differential equations. Indeed, finding the numerical solution of the Navier-Stokes equation is increasingly difficult when the solid boundary condition ceases to conform to simple shapes. An alternative computational approach is therefore needed (e.g., Galdi 1994, Fergizer 1999), from which to develop a three-dimensional model for the flow and phytoplankton transport around mussels.

3.2 The Cellular Automaton Approach

Cellular Automata are simulation systems, invented in the late 1940s by John von Neumann and Stanislaw Ulam (e.g., Taub 1963, Toffoli and Margolus 1987). They have three properties: space, information and law. Space is represented by a uniform grid of cells and spans a given number of dimensions, with a specified geometry. Each cell contains information, expressed either as quantities, states or a combination of both. Time advances in discrete steps as the entire system is updated simultaneously, in accordance with the universal law. It is therefore a discrete dynamical system. The law is an update rule that determines the new data in each cell, either deterministically or stochastically. The rule is expressed as a function of a cell's current information and that of its neighbours. Conventional Cellular Automata have the properties of homogeneity and locality, the latter suiting them extremely well to parallel computing. A good introduction to the Cellular Automata modelling environment may be found in Toffoli and Margolus (1987).

In 1970, a mathematician at the University of Cambridge named John Conway introduced a Cellular Automaton rule in which simple patterns could grow arbitrarily large (Gardner 1970). This system, entitled 'Life', simulated growth, death and reproduction, and was therefore conjectured to simulate biological processes. 'Life' predictably caught the attention of biologists and kindled a public interest in Cellular Automata.

Since then, Cellular Automata have been applied to many and varied avenues of complex systems science, possibly the most successful application being fluid flow. This area of research has brought about the introduction of Lattice Gas Automata (LGA), which build on the basic cellular concepts. The FHP Lattice Gas model, named after inventors Frisch, Hasslacher and Pomeau (Frisch et al 1986), was very successful, due to the isotropy maintained in the lattice structure. Simultaneously, this hexagonal structure was utilised by Stephen Wolfram (Wolfram 1986), who patented Lattice Gas models. Research on Lattice Gas Automata (Wolfram 1994, Rothman and Zaleski 1997) has developed to include integer (Boghosian et al 1997) or multiparticle (Masselot and Chopard 1998) fluid representation.

This avenue of modelling has been pursued in this course of research, to the extent of developing an LGA hydrodynamic model for simulation at the first scale of consideration, water flow past a cluster of mussels. However, the LGA approach was subsequently abandoned, due to a combination of technical limitations and the unsuitability of the LGA simulation environment to modelling requirements (See Appendix A).

Recently, the Lattice Boltzmann (LB) method has advanced as a development of Lattice Gas Automata, providing a solution to the problems that were encountered with LGA. The LB method is based on the Boltzmann equations and relates local angular distribution of momentum to local density and velocity. It allows easier implementation and more complex boundaries than the Finite Element Method (FEM). The LB method is capable of generating Navier-Stokes behaviour (Giraud and Popinet 1994, Martys 2001) and compares well with FEM performance (Kandhai et al 1998). Thus, the selection of LB modelling for this task seems natural.

First, detail on the theory behind the LB method (Giraud and Popinet 1994, Filippova and Hanel 1997, Chen and Doolen 1998, Xi et al 1999) is given.

3.3 Lattice Boltzmann Theory

The distribution of fluid momentum at each vertex of the LB grid is expressed as a vector, F, containing n elements, where n is the number of links to adjacent vertices. This vector may also be considered as the probability distribution over the directions that a unit of fluid may travel in the next time step, connected by the normalising density scalar, ρ. As time is iterated, the fluid is updated according to homogeneous rules simulating advection, reflection and collision. Units of fluid are displaced according to the distribution vector, some simultaneously bounce off solid boundaries. The fluid interaction process is defined by a collision operator, Δ, which forces local distribution functions to approach equilibrium states. The underlying equation is:

$$F_i(X + e_i, t + \delta_t) = F_i(X,t) + \Delta_i[F(X,t)], \tag{5}$$

where $i \in \{1,...,n\}$, e_i is the lattice vector in direction i, X is the variable spatial vector, t is the temporal variable and δ_t is the incremental time step.

For given local fluid properties such as mass and momentum, there is an unique equilibrium distribution function. This function is the truncated version of the standard Maxwellian distribution used in Statistical Physics. In its general form it is expressed as:

$$F_i^{eq} = c_1 + c_2(V \cdot e_i) + c_3(V \cdot e_i)^2 + c_4|V|^2 \tag{6}$$

where V is the local velocity vector. The coefficients c_1 to c_4 depend on the lattice index i, and are obtained from conservation laws, to ensure

$$\sum_{i=1}^{n} F_i^{eq} = \rho \tag{7}$$

and

$$\sum_{i=1}^{n} e_i F_i^{eq} = \rho V , \tag{8}$$

where ρ is the fluid density. The second and third moments are also required here, so that F^{eq}, having four coefficients, can be specified uniquely. The final constraint, incorporating the third moment, requires lattice isotropy. This therefore becomes a key issue in grid selection, which will be discussed in the next section.

This distribution is the steady state for fluid momentum with those particular density and velocity values. It is therefore possible to represent local fluid momentum in equilibrium and non-equilibrium components:

$$F = F^{eq} + F^{neq}, \tag{9}$$

the latter having zero mass and momentum.

The collision operator is then applied to the non-equilibrium component, in the form of the operator, Ω, so that mass and momentum are unaffected,

$$\Delta(F) = \Omega(F^{neq}) = \Omega(F - F^{eq}) . \tag{10}$$

A construction method for the operator Ω is to linearise it into an n by n collision matrix, since F^{neq} is a vector of n elements. If the eigenvalues of Ω are large and negative, Δ will have the effect of quickly restoring the local distribution function to equilibrium, that is, to F^{eq}. In this way, the viscosity of the fluid is determined by the eigenvalues of Ω, so that viscosity may be specified directly as a free parameter in the LB system.

A full derivation of the Navier-Stokes equation from the Lattice Boltzmann formulation, using a Chapman-Enskog expansion technique, is given in Hou et al. (1995).

3.4 Implementation of the Lattice Boltzmann Model

The LB model acts on a regular grid, or lattice. It is imperative that the chosen lattice is isotropic, that is, fluid behaviour will not depend on the orientation of the grid. In particular, LB theory given in the previous section requires lattice isotropy according to the following definition.

Let $\{e_i\}$ $i \in \{1...n\}$ be a set of n vectors and η be a variable vector.

Let

$$I_K = \sum_{i=1}^{n} (e_i \cdot \eta)^K , \tag{11}$$

the K^{th} lattice tensor, be a function of η.

A lattice grid based on the set $\{e_i\}$ is isotropic if

$I_K = 0$ for all odd K and

I_K is independent of η for K=2 and K=4.

The set associated with the basis vectors from the Cartesian coordinate system does have constant I_2 for all dimensions. However, I_4 is not independent of η in this system. Full isotropy is possible in two dimensions through utilisation of a hexagonal grid, as is employed in FHP Lattice Gas Automata. Unfortunately, there is no three dimensional analogy for this, in fact, there is no isotropic coordinate system in three dimensions at all.

There is, however, an isotropic vector set which spans four-dimensional space. The grid based on this set is known as the face centred hyper cubic (FCHC), defined by the 24 vectors in four dimensions that have Cartesian coordinate entries 0 or 1 and magnitude

$\sqrt{2}$. Each vector represents the link to a grid point adjacent to the origin. The Lattice Boltzmann system is constructed for this FCHC grid, applying the principle that any lower dimensional space can be viewed as a cross section of a four dimensional space, related by a projective operator. See Benzi et al. (1992) and Wolfram (1986) for details on the collision matrix based on the FCHC lattice.

The terms 'grid point', 'site' and 'cell' are used in similar contexts in this thesis. The formal definition of a cell is therefore given, via the standard Wigner-Seitz constructive algorithm:

1. Choose any lattice site, or grid point, as the origin.
2. Beginning at the origin, construct vectors to all adjacent lattice points. In the case of the face centred hyper cubic, these are the 24 mentioned previously.
3. Construct a hyperplane perpendicular to and passing through the midpoint of each vector.
4. The area or volume enclosed by these hyperplanes is the Wigner-Seitz cell.

The elements of Ω for any particular grid is dependent on the angle θ between the vectors in that grid. There are only five possible values for θ in the face centred hyper cubic, these being 0, 60, 90, 120 and 180 degrees. The elements of the collision matrix are denoted by ω_0, ω_{60}, ω_{90}, ω_{120} and ω_{180}, combinations of which are directly related to physical conservation laws. In particular, local fluid mass is conserved if and only if

$$\omega_0 + 8\omega_{60} + 6\omega_{90} + 8\omega_{120} + \omega_{180} = 0. \tag{12}$$

Similarly, local momentum is conserved if and only if

$$\omega_0 + 4\omega_{60} - 4\omega_{120} - \omega_{180} = 0. \tag{13}$$

Aspects of the system, namely the grid, distributions and operators, can be projected onto lower dimensional systems. A simple way to project vectors is to express them in Cartesian co-ordinates, then truncate the final elements. Applying this projection to the FCHC grid produces the 18-direction model in three dimensions and the 8-direction model in two dimensions. For computational purposes, projection is expressed through formation of a binary matrices P_2 and P_3.

The equilibrium distribution is similarly projected to lower dimensions. For example, its three-dimensional form is

$$F_i^{eq} = w_i\left(1 + 3(V \cdot e_i) + 4.5(V \cdot e_i)^2 - 1.5|V|^2\right) \tag{14}$$

where w_i =

$$\begin{aligned} &1/3 \quad \text{for} \quad e_i = (0,0,0), \\ &1/18 \quad \text{for} \quad e_i = (\pm 1,0,0),(0,\pm 1,0),(0,0,\pm 1), \\ &\text{and} \quad 1/36 \quad \text{otherwise.} \end{aligned} \tag{15}$$

Similarly, the new Collision matrix can be found by

$$\Omega_3 = P_3 \Omega_4 P_3^{-1} \tag{16}$$

where the pseudo-inverse suffices for P_3^{-1}, since non-uniformity of flow across the fourth dimension is unnecessary.

Overall momentum of the system is imposed and maintained on the boundary of the grid by essentially forcing a velocity differential on whichever row or column of the lattice represents the upstream edge of the domain. Uniform flow is simulated by imposing a constant momentum vector.

It is important to note that the projection of the original Wigner-Seitz cell is not equal to the Wigner-Seitz cell calculated for the projected grid. Cells in the projected systems are therefore considered merely as units of identical volume (or area), centred at their respective grid points, that is, the Cartesian lattices in two and three dimensions. Secondly, lattice vectors are no longer of equal magnitude under this projection. The original system isotropy is not lost due to these observations, however, since it is dependent on the LB construction for the higher dimensional grid.

In this sense, the Cartesian lattice may be employed to specify the solid boundary. The array M representing the solid boundary, that is, the cluster of mussels, is binary. Cells are either fluid or solid, denoted by $M = 0$ and 1 respectively.

This means that there exist two adjacent cells X_i and X_j, where $M(X_i) = 0$ and $M(X_j) = 1$. The true edge of the mussel passes through the midpoint of X_i and X_j. So, in one iteration, momentum centred around X_i, directed towards X_j, should end up centred around X_i after advection and reflection. It is also important that reflection is reversible. If momentum is redistributed between two distinct cells after reflection, a measure of diffusion has occurred, which is undesirable from a physical perspective.

Secondly, the numerical velocity field near a boundary must represent the true behaviour of the fluid there. Consider a zero-velocity scenario, with $X_i<X_j$. If reflection occurs before advection, there will be no resultant negative component of momentum at X_i. This will be erroneously interpreted as a non-zero normal velocity at the boundary. Also, if reflection occurs after advection, no positive momentum is permissible at X_i, because advection is not defined adjacent to, and normal to, a boundary. To resolve these issues, it is necessary that advection and reflection occur simultaneously, in the following manner:

$$F_i(X + e_i, t + \delta_t) = F_i(X, t) + F_{\tilde{i}}(X + e_i, t)M(X) \tag{17}$$

where $\tilde{i}$ and i are connected by the relationship $e_{\tilde{i}} = -e_i$.

In each iteration, it is important that the various processes, functions and operations occur in a workable sequence. The scheme:

1. Imposition of velocity on grid boundary
2. Fluid development, involving advection and reflection
3. Local LBM collision function

is derived from the level of homogeneity within each step. For example, implementing the velocity is highly inhomogeneous, ranging to the equilibrium and collision step, which is applied to every cell of fluid in the entire grid.

3.5 Tests

To validate the implementation and coding of the LB model (see Redhead 1980, Oreskes et al. 1994), numerical results will first be compared with analytic solutions of the time decay of fluid velocity. Second, simulations will reproduce a well known and measured relationship between Reynolds number and drag coefficient of submerged cylinders.

It is established that fluid viscosity may be derived from the LB operator construction (e.g., Succi et al. 1991, Chen and Doolen 1998). Alternatively, it may be calculated from simulations of a known analytical solution involving fluid viscosity, ν. To apply this approach, the velocity profile in the model is set to:

$$V_x = A_0 \sin(y)$$
$$V_y = V_z = 0 \qquad (18a,b)$$

at an arbitrary amplitude A_0 and left to diffuse.

In the absence of external forces, velocity fields are known to diffuse according to the simplified Navier-Stokes equation

$$\frac{\partial V}{\partial t} = \nu \nabla^2 V \tag{19}$$

which, in this situation, gives

$$V_x = A(t)\sin(y) \tag{20}$$

with

$$A(t) = A_0 \exp(-\nu t)\,. \tag{21}$$

That is, the amplitude A of the sine wave decays exponentially over time. A numerical value for ν is obtainable by calculating the slope of the best linear fit between t and $\log(A)$.

Comparison of these independent viscosity values, from theory and from simulations, showed agreement, as shown in Figure 2.

The second test problem relates to a well-established relationship between Reynolds number Re and drag coefficient C_d in flow past a cylinder (e.g., Tritton 1988, Faber 1995), which is utilised to test the model. A good example of exploring this problem with computational tools is presented in Tutar (2001). In our test the fluid force is calculated first from summation of particle reflection off the cylinder; the obtained value of this force is then used to compute the drag coefficient. Thus, the relationship $C_d = C_d(\mathrm{Re})$ from simulations was compared with that obtained from physical experiments.

The comparison between the measured and experimental curves is shown in Figure 3. Simulations at particular Reynolds numbers were run with more than one combination of velocity and diameter. That these independently generated data collapsed onto the same curve is a positive result from this numerical experiment. The overall accrement in curve shape also serves to validate the model. The variance between the numerical and empirical curves of drag coefficient (taken as percentage differences) entails a root mean

square error of 18%, due to high drag values at low Reynolds numbers and low drag values at high Reynolds numbers. This error is not solely the result of the flow model used, but is also due to the representation of a cylinder on a discrete grid. In particular, if the discretization of the cylinder translates into a form of surface roughness, then low drag values are precisely what would be expected at high Reynolds number flows.

The LB method deployed in both of these test problems involved a 200 by 200 lattice, simulating incompressible flow with pressure a constant multiple of density. The maximum fluid speed in both experiments corresponded to a Mach number of $\sqrt{3}/100$.

3.6 Inclusion of Biophysical Processes

This section details the development of the model to include physical processes such as the diffusion and advection of phytoplankton (e.g., Denman and Gargett 1995). Methodology will also be outlined for incorporating the geometry of each mussel into the model and for simulating the physiological process of plankton filtration by the mussels. It is proposed that the dynamic nature of the model be retained, for the inclusion of these biophysical aspects.

Superimposition of such quantities subject to advection and diffusion is made easier by the fact that the grids in both two and three dimensions have a Cartesian substructure. The water velocity vector can be obtained for each node of the lattice from manipulation of Equations 7 (p20) and 8 (p21) for density and momentum:

$$V(X) = \frac{\sum_{i=1}^{n} e_i F_i(X)}{\sum_{i=1}^{n} F_i(X)} \qquad (22)$$

Instantaneous velocity profiles from the LBM can therefore be imported into the next phase of modelling, where the plankton concentration, C, evolves separately and discretely, according to the advection/diffusion partial differential equation

$$\frac{\partial C}{\partial t} = D\nabla^2 C - V \cdot \nabla C \tag{23}$$

with

$$\begin{aligned} \nabla^2 C(X) &= \frac{d}{n}\sum_{i=1}^{n}\frac{\partial^2 C}{\partial X_i^{\,2}} \\ &\approx \frac{d}{nl^2}\sum_{i=1}^{n}\left(C(X+e_i) - 2C(X) + C(X-e_i)\right) \\ &= \frac{2d}{nl^2}\sum_{i=1}^{n}\left(C(X+e_i) - C(X)\right) \end{aligned} \tag{24}$$

and

$$\begin{aligned} \nabla C(X) &= \frac{d}{n}\sum_{i=1}^{n} e_i \frac{\partial C}{\partial X_i} \\ &\approx \frac{d}{nl}\sum_{i=1}^{n} e_i\left(C(X+e_i) - C(X)\right) \end{aligned} \tag{25}$$

where d is the number of dimensions spanned by the vectors e_i and l is the spatial step.

The implementation of mussels into the model as solid boundaries is not trivial. It would be very difficult to approximate the geometry of a mussel with a combination of analytic surfaces from ellipses, cones and planes, all represented numerically. It is possible, however, to make use of the cellular nature of the model (See discussion on cells in Section 3.4) by utilising digital photographs of a typical mussel (Figure 4). These images are analysed and converted into a three dimensional binary array, allowing scaling and rotation (Figure 5).

It is beyond the scope of this model to simulate the internal hydrodynamics of the mussel, which is not yet clear (e.g., Barker and Jorgensen 1996). However, it is necessary that physiological processes be represented to some extent. Mussels inhale plankton-rich

water and exhale plankton-depleted water at some other point on the mussel. The velocity of this interior filtration current is calculated from established physiological data (Riisgard and Mohlenberg 1979, Meyhofer 1985, Best 1988) of the volumetric filtration rate, which is approximately 5 litres per hour per individual mussel.

The filtration velocity, V_f, can be deduced using the equation

$$V_f = \frac{R}{l^2}, \tag{26}$$

where R is the volumetric filtration rate and l^2 is the cross-sectional area through which water is siphoned. This current is imposed in the hydrodynamic phase of modelling.

In order to avoid hydrodynamic inconsistencies in simulation of this process, a tunnel is hollowed from the inhalant to the exhalent point of the model of the individual, with a forced velocity throughout. This is to avoid the loss in continuity at the mussel surface that would be created if a velocity was imposed on the exterior of the mussel only.

As the water passes through a mussel, its plankton content is set to zero, to simulate the filtration process. The present model does not account for other biological aspects such as pseudofaeces production or other influences of varying particulate concentrations.

The ambient plankton concentration is maintained on the upstream side of the model grid, along with upstream velocity. Only the relative plankton concentration is considered, so that unit concentration is implemented on the boundary at each time step.

Chapter 4 - SMALL SCALE SIMULATION

This chapter details the first stage of simulation of mussel arrangements and the question of optimality at this smallest scale. As discussed previously, the arrangement of mussels on a section of rope will be varied, as well as the diffusion coefficient value and the orientation of the rope to the flow.

In first addressing the configuration of mussels, an apparent difficulty is how it might be quantified. The structure of mussels on a rope section is not easily represented by a real number. Under optimality considerations, however, configurations are more usefully expressed in comparison with the most dense arrangement of mussels possible, which is in turn highly dependent on the geometry of a single mussel. Thus, the question arises of how densely mussels can be packed.

4.1 A Physical Model

A physical model was constructed, in order to ascertain how many mussels can fit radially around a rope and how many layers of these radial sets of mussels fit along a set length of a rope section. The model included mussel shells, attachable onto a stretch of rubber resembling the dimensions of a rope. Mussels were attached from their endpoints, pointing outwards, in the manner of natural formation. It was found that six mussels would fit around the rope and another six mussels, rotated 30 degrees relative to the original six, could fit above them, with a slight vertical overlap. This unit of twelve mussels can be repeated up or down the rope, again with the same slight vertical overlap. It was found that the thickness of one mussel unit (twelve mussels) is on average 0.044 m, giving a total mussel density of approximately 273 mussels per metre.

On a grid of 55x55x55 cells, with each mussel scaled to 16 cells in length, a total of 60 mussels, arranged in five layers, can be placed in this full configuration. This provides grid resolution of l = 0.004 m. The occupation of each of these five layers is a measure of density, giving a means for quantifying mussel arrangement. The model is designed with periodic boundary conditions, with the result that the top of the computational domain is connected with the bottom, making the rope potentially infinite in length.

Once these mussel clusters have been introduced into the model (Figure 6), they become the solid boundary for the hydrodynamic phase of modelling with the LB method. Running the model, with this full configuration of mussels, produces velocity (Figure 7) and plankton fields (Figure 8). The small areas of turbulent behaviour behind the mussels are evident, as are the downstream zones of plankton depletion.

4.2 Mussel Density Effects

Five layers of mussels provide an initial scope of 32 possible configurations, within which the cluster density can be varied. However, these reduce to 8 when taking the infinite nature of the grid into account, since many configurations are longitudinal displacements of each other, so may be considered under the same equivalence class. The 8 configurations (defined as Cases) are:

1. 0 layers (trivial and non-simulated case)
2. 1 layer
3. 2 layers adjacent
4. 2 layers non-adjacent
5. 3 layers with the remaining gaps adjacent
6. 3 layers with the remaining gaps non-adjacent
7. 4 layers
8. 5 layers

For each Case, the characteristics of the collective phytoplankton uptake were studied, in particular the mean of the individual uptake rates. Note that the terms uptake and uptake rate are used interchangeably here, since the only concerns at this stage are equilibrium states and relative phytoplankton quantities.

The simulations showed that Case 2 and Case 4 produced the highest mean uptake and that Case 8 produced the lowest mean uptake. Figure 9 demonstrates how the mussel density influences the mean uptake. The visible non-linear effect of plankton uptake is a consequence of the mussel competition for the plankton. The mussels generate local zones of plankton depletion, so that, when mussels are too close together, there is decreased food potential for downstream mussels. This non-linear effect compounds wherever two mussels are in each other's depletion zones.

Additional information may be extracted from the comparisons between Case 3 and Case 4, also between Case 5 and Case 6, since these represented changes in arrangement, with density held constant. Consistently, the configuration with less clustering yielded better results, that is, Case 4 and Case 6 produced higher uptake means.

4.3 Sensitivity to Diffusion

As mentioned, simulations were conducted with diffusion coefficient values of 0, 10^{-5}, 10^{-4} and 10^{-3} m^2/s. This section focuses on the effect that the diffusion rate has on both the uptake of the mussels and on the identification of the optimal structure. The domain of structures for experimentation at this scale is limited to Cases 3 and 4, in order to obtain a qualitative understanding of the governing dynamics.

Figure 10 indicates that the uptake mean is a decreasing function of the diffusion coefficient, but that this decrease is minimal considering the range of coefficient values. Case 4 gives consistently higher uptake (circles) than Case 3 (crosses), but the difference

between Case 4 and Case 3 becomes negligible as diffusion reaches the high end of the diffusion domain, 10^{-3} m^2/s.

4.4 Orientation and Drag

In all simulations, the rope has been perpendicular to the water flow. However, it may be necessary or desired for the base unit in subsequent scales to be orientated differently (e.g., Bushnell and Moore 1991, Vogel 1994). To gauge the effect of varying the orientation of the full cluster to the flow, simulations were conducted with the imposed boundary velocity at other angles to the rope, namely parallel ($\theta = 0$ and $\theta = \pi$) and oblique ($\theta = \pi/4$ and $\theta = 3\pi/4$). The need for this further distinction within parallel cases and oblique cases is due to the orientation of the mussels on the rope and, more importantly for the uptake simulations, the direction of the filtration current forced by each mussel. The angle θ, in addition to representing the angle of the rope to the flow, also represents this filtration angle, relative to the flow. Statistics were recorded for uptake rates and the measured drag force for the body, for each of the 5 cases.

Results for the set of 60 uptake rates are outlined in Table 1.

Table 1: Uptake at Various Orientations to the Flow

θ	0	$\pi/4$	$\pi/2$	$3\pi/4$	π
Mean	0.6285	0.8369	0.9671	0.8164	0.5823
Variance	0.0797	0.0684	0.0055	0.0721	0.0805
Q/N	0.2816	0.6305	0.9353	0.6072	0.2730

In order to generalise these results in a theoretical framework for later scales, the mean of the individual uptake rates, as a measure of efficiency, is considered as representative of

all three of the statistical properties given in Table 1. Details on its theoretical treatment required for later assimilation is therefore given.

The data points relating to the means of uptake rates can be interpolated with a specified function on the closed interval $(0,\pi)$. This function will provide parameters for modelling at later scales.

It is first observed that such a function, f, will be periodic with period 2π and symmetric around $\theta = 0$ and $\theta = \pi$. The function f is therefore asserted to be a series of cosine terms, up to fourth order in this case, since there are 5 data points. It is expressed in the form

$$f(\theta) = \sum_{i=0}^{4} c_i \cos(i\theta). \tag{27}$$

The coefficients c_i are deduced from the values for the mean uptake rate, listed in the above table, to give the continuous function as seen in Figure 11.

The drag force, due to the water pressure, on the cluster of mussels, was calculated at various orientations to the flow. The following results were obtained, with force measured in Newtons and θ in radians from parallel to the flow:

Table 2: Force at Various Orientations to the Flow

θ	0	$\pi/4$	$\pi/2$	$3\pi/4$	π
Force	0.18	0.34	0.33	0.33	0.18

With the same approach used for the mean uptake rate data, these points can be interpolated by a continuous function, a sum of cosine curves (Figure 12).

It is seen that there is a high level of drag over a wide range of θ near $\pi/2$, where the rope is near perpendicular. Since drag force is not included in the optimisation objectives, the fact that perpendicular ropes incur large drag does not affect the preference for that orientation from this point onward. However, these results will be utilised in higher scales to the extent that orientation, and therefore drag, variation will affect momentum loss in the surrounding volume of water.

4.5 Discussion of Mussel Density, Diffusion and Orientation Effects

In varying the arrangement of mussels, it was found that there is a non-linear reductive effect on plankton uptake, observable as the cluster density is increased. Comparisons between intermediate cases that have the same density demonstrate the extent of this non-linear effect. However, uptake reduction was not sufficient to justify abandonment of the fully occupied configuration as the optimal structure for the first scale of modelling. This is because that arrangement, Case 8, performed the most efficiently, under Criteria B and C, especially considering the mean of uptake rates, as also mentioned in Section 2.1. Case 8 is also trivially optimal under Criteria A, since it is the only configuration with 60 mussels.

The diffusion of phytoplankton, although easily tuneable in a numerical sense, gives results that have relevance in two distinct areas. Firstly, the sensitivity of the model to diffusion is quantified, in the sense of its input as a physical constant. Secondly, for larger scales, for instance when considering the position of a farm within a bay, environmental conditions such as plankton diffusion do change. They may also fluctuate significantly in the time domain (e.g., Nikora et al. 2002c, Stevens 2003). In this context, it is useful to retain results from different values of diffusion. Increasing the diffusion rate generally decreases plankton uptake. This is because the scope of the depletion zones is widened to encompass other mussels. The effect of increased diffusion would be reversed if mussels were arranged so that some could not access plankton to the same extent. Therefore, the observed trend is a positive outcome. Another result is the lack of preference for optimal

arrangement in high diffusion scenarios, where the Péclet number is low. Such a result is expected, since increased diffusion decreases the dependence on mussel location.

The primary result for this scale of simulation is that the fully occupied configuration is found to the most efficient, after considerations of cluster density and plankton diffusion. Uptake statistics have also been obtained which will, along with drag coefficient calculations, provide the necessary parameters for large-scale modelling, where small scale turbulent effects and individual mussel geometries are inconsequential.

In consideration of these statistics, in particular, this chapter is concluded with some further analysis of the uptake data from the optimal configuration.

4.6 Uptake Distribution

In the above sections, results related to the bulk characteristics of uptake rate were presented. However, the statistical distributions of individual uptake values for a given mussel cluster may provide a better description of system behaviour. This would also give the ability to calculate specific percentile values, rather than merely a mean or total.

Here Case 8 is considered, which has demonstrated the most effective performance under all sets of criteria. Simulations were conducted with the diffusion coefficient of 10^{-5} m^2/s, for an ensemble of mussel clusters of the same Case 8, where each cluster was slightly different from others. This difference entailed small variation in the horizontal positions of mussels, so that adjacent layers were not directly below one another. The spatial variation consisted of displacing a layer by 1 grid unit in each of the dimensions perpendicular to the rope. This gives 4 possible positions for each layer. These possible positions, applicable to all 5 layers, provide a large population base from which a large data sample was generated randomly.

The obtained probability density function of individual uptake rates (Figure 13) was found to be highly negatively skewed, to the extent that the mode seems to coincide with the maximum. The primary application of this observation is that percentiles are abnormally high in comparison with the mean.

In seeking to describe this distribution of individual uptake rates, it is intuitive to hypothesise that this density function may be derivable from independent theoretical means.

With this in mind, consider an arbitrary set of mussels in plankton-filled flow. As an approximation to the depletive effect of the upstream mussels, it is assumed that, given any set of mussels, a certain proportion of them will be located in water which is depleted of plankton, due to the remainder. A second assumption is that this proportion, p, is independent of the shape of the mussel set.

So, defining N as the number of mussels present, pN will have uptake rates decreased to less than some second proportion, q, of the maximum attainable rate. Now, considering these pN mussels as a set, the same reasoning applies, giving the second level of uptake reduction. That is, p^2N mussels will uptake plankton at a rate less than q^2. This concept extends indefinitely, implying that p^iN mussels uptake at a rate less than q^i.

To generate $f(u)$, where u is the uptake rate and f is the density function, it is observed that

$$f^C(q^i) = p^i \tag{28}$$

where ^{C} indicates the cumulative frequency.

Eliminating i as a redundant parameter leads to $f^C(u) = u^\gamma$, with $\gamma = \dfrac{\log(p)}{\log(q)}$, giving

$$f(u) = \gamma u^{\gamma-1}. \tag{29}$$

Further application of this analysis is that, since power curves are defined by a single parameter, γ, only one measure of uptake is required; the rest may be theoretically deduced. For example, the proportion of uptake rates that are above proportion q can be estimated, with the following consideration. It is known that the mean is directly related to γ according to

$$\mu = \frac{\gamma}{\gamma + 1}. \tag{30}$$

Similarly, Q/N can be found to be

$$Q/N = 1 - u_0^{\gamma} = 1 - 0.8^{\left(\frac{\mu}{1-\mu}\right)}. \tag{31}$$

Secondly, if the ambient plankton concentration is reduced by a scaling factor r ($0.8 \le r \le 1$), the mean and variance are trivially scaled down by r and r^2 respectively. The new $Q/N_{(r)}$ can be estimated from the old Q/N value, with the relationship

$$Q/N_{(r)} = 1 - \frac{1 - Q/N}{r^{\gamma}}. \tag{32}$$

A second possibility for expressing the uptake distribution analytically comes with the possibility that there is only an apparent mode at 1 in the uptake rate distribution. The real data may be spread much more Normally than a power curve would imply. A Normal curve, however, is defined on the entire real line. A conjecture is given for the probability distribution by applying a map from the open interval (0,1) to the real line and suggesting that the mapped data is approximately Normal. A theoretic distribution for f on the interval can then be found by applying the inverse of the map to a perfectly Normal distribution.

The function

$$g(u) = \log\left(\frac{u}{1-u}\right), \tag{33}$$

provides such a map. The skewness of the mapped data, -0.55, is relatively negligible, which supports this approach. The mean and standard deviation of the data are 4.03 and 1.38 respectively, which become the parameters for the fitted Normal curve (Figure 14).

Chapter 5 – MEDIUM SCALE SIMULATION

Results from simulations at the smallest scale provide parameters for this next scale of modelling. Variations will be introduced in the structural arrangement of the mussel set and in the flow conditions. It is unfeasible to vary, simultaneously, all of the independent parameters from the first scale, in addition to these new ones. The density of mussels within a cluster will therefore be held at 60 mussels per 0.22 m unit of rope, as determined by decisions on optimality in the previous chapter. The plankton diffusion coefficient will be kept at the typical value of 10^{-5} m^2/s, since the computational results were not sufficiently sensitive to this value, at the first scale, to necessitate its continued variation.

This chapter gives results from various approaches toward optimality at the medium scale of consideration. Methodology behind the simulation used for these approaches is given. Results are presented first for the efficiency of simple arrangements, then an algorithm is given for generating potentially optimal structures under various flow conditions. Intuitively designed structures are discussed; efficiencies of these arrangements are compared. Finally, the issue of optimality for unconnected arrangements is addressed and an algorithm for improving the efficiency of any given arrangement is presented and discussed.

5.1 Construction and Theory

Until this point, simulations have involved embedding the structure into a hydrodynamic model until spatial dynamics attain an equilibrium velocity profile, then superimposing phytoplankton dynamics onto that flow field. A property of this next scale, however, is that the grid increments are relatively large, so that the hydrodynamic influence between occupied units is assumed to be negligible. It will become apparent that this makes a

large part of the simulation methodology redundant, beyond initial field generation for each flow condition. This will increase computational speed, giving scope for a larger number of simulations.

The hydrodynamic/plankton model will first be run with only one occupied unit. The depletion of plankton and drag force on the water in this unit are forced using data from the previous scale. The local plankton concentration is reduced at a constant rate, which depends on the volume of the unit. The local water velocity is affected by the drag force, which was also measured in the small scale of modelling. This reduction in local speed will be counteracted by the viscous forces from the surrounding water, so that the speed will converge on an equilibrium value. These update rules are added to the hydrodynamic model. By simulating filtration and drag in this way, a discrete field of plankton concentration is obtained, showing the downstream depletion zone caused by that unit, located at the origin (Figure 15). The field caused by a vertical string of units can also be generated (Figure16).

Since plankton uptake is linearly dependent on plankton concentration levels, a second unit, configured and orientated identically, situated downstream from the first, will uptake at a rate proportional to the observable plankton levels at that location in the generated concentration field. Secondly, the combined hydrodynamic field is merely an addition of the two equivalent fields. The outcome of including a second unit downstream can therefore be predicted.

If the second unit is situated close to the original, such that it affects the uptake of the original, the two units will be interdependent. A dynamical systems approach can be employed, to find the steady state uptake rates of the two units, instead of needlessly applying the hydrodynamic model for the new arrangement. This is easily generalised to N interdependent units. Each has an ideal uptake of 1, diminished by each of the others, depending on its respective displacement from those other units. This decrease can be found by the plankton field, generated from a single unit at the origin, or more

specifically, from $h(X)$, which measures the decrease from 1 of that plankton concentration field.

Let X_i be the location of the i^{th} unit; let u_i be the uptake rate of that unit. As time evolves,

$$u_i \rightarrow 1 - \sum_{j \neq i} h(X_i - X_j) u_j \,. \tag{34}$$

Considering u as an N x 1 vector of uptake rates, and introducing H, where

$$H(i,j) = \begin{cases} h(X_i - X_j) & j \neq i \\ 0 & j = i \end{cases}, \tag{35}$$

the iterative map (34) can be expressed in vector form as

$$u \rightarrow 1_N - Hu \tag{36}$$

where 1_N is an N x 1 vector of ones. Since the elements of H are small, u quickly approaches equilibrium

$$u^{eq} = (I + H)^{-1} 1_N \tag{37}$$

which is equivalent to the row-sum of $(I + H)^{-1}$. This inverse can be approximated by a truncation of its expansion. It was found that sufficient accuracy can be obtained with the fourth order estimate:

$$I - H + H^2 - H^3 + H^4, \tag{38}$$

which can be regrouped as *I-H(I-H(I-H(I-H)))* for more efficient coding.

Following this methodology, all that is needed to obtain the uptake of N units are their co-ordinates and the plankton field generated from 1 unit. It should be noted that the co-ordinates of the N units need not sit on the same grid of resolution 0.22m. Linear interpolation allows h to be calculated at any real-valued co-ordinates. Further, h approaches 0 in all directions away from the origin, so there is no need for all of the N units to be within the domain of the generated plankton field. That is, $H(i,j)$ is simply assumed to be 0 when $X_i - X_j$ is outside a certain volume.

Once u^{eq} is obtained, the combined distribution of individual uptake rates can be found, using the distribution within 1 unit, from the previous Section. The total data set consists of N sets of data, where the i^{th} set is the original 60 values, multiplied by u_i.

The theory derived in Section 4.6 can be continued by considering the analytical distribution of this combined data set.

The original data set from small scale modelling, distributed according to $f_1(u_1)$, will produce the distribution

$$\frac{1}{u_2} f_1\left(\frac{u_1}{u_2}\right) \tag{39}$$

when multiplied by a single value of u_2.

Further, the medium scale set will be distributed according to some function $f_2(u_2)$, so that the combined total data set will have a distribution

$$f(u_1) = \int_{u_2=u_1}^{1} \frac{1}{u_2} f_1\left(\frac{u_1}{u_2}\right) f_2(u_2) du_2 \,. \tag{40}$$

If these distributions follow a power law, as mentioned in Section 4.6, the new distribution and its associated statistical properties can be found analytically.

Let $f_1(u_1) = \gamma_1 u_1^{\gamma_1 - 1}$ and $f_2(u_2) = \gamma_2 u_2^{\gamma_2 - 1}$ with $\gamma_1, \gamma_2 \neq 1$. Then,

$$\begin{aligned} f(u_1) &= \gamma_1 \gamma_2 \int_{u_2 = u_1}^{1} u_1^{\gamma_1 - 1} u_2^{\gamma_2 - \gamma_1 - 1} du_2 \\ f(u_1) &= \frac{\gamma_1 \gamma_2}{\gamma_2 - \gamma_1} \left(u_1^{\gamma_1 - 1} - u_1^{\gamma_2 - 1} \right) \end{aligned} \tag{41}$$

provided $\gamma_1 \neq \gamma_2$.

The new mean and variance are

$$\mu = \frac{\gamma_1 \gamma_2}{(\gamma_1 + 1)(\gamma_2 + 1)} \tag{42}$$

and

$$\sigma^2 = \frac{\gamma_1 \gamma_2 (\gamma_1^2 + 2\gamma_1 + \gamma_2^2 + 2\gamma_2 + 1)}{(\gamma_1 + 2)(\gamma_2 + 2)(\gamma_1 + 1)^2 (\gamma_2 + 1)^2} \tag{43}$$

respectively. Also, there is a mode at

$$u_1 = \left(\frac{\gamma_1 - 1}{\gamma_2 - 1} \right)^{\left(\frac{1}{\gamma_2 - \gamma_1} \right)}. \tag{44}$$

The special case, $\gamma_1 = \gamma_2 = \gamma$, gives

$$\begin{aligned} f(u_1) &= \gamma^2 \int_{u_2 = u_1}^{1} u_1^{\gamma - 1} u_2^{-1} du_2 \\ f(u_1) &= -\gamma^2 u_1^{\gamma - 1} \ln(u_1) \end{aligned} \tag{45a,b}$$

which has a mean of

$$\mu = \frac{\gamma^2}{(\gamma + 1)^2}, \tag{46}$$

a variance of

$$\sigma^2 = \frac{\gamma^2(2\gamma^2+4\gamma+1)}{(\gamma+2)^2(\gamma+1)^4}, \tag{47}$$

and has a mode at

$$u_1 = \exp\left(\frac{-1}{\gamma-1}\right). \tag{48}$$

5.2 Flow Conditions

Earlier simulations were run with uniform flow, on the assumption that circulation and tidal periodicity has effect only at larger time scales and, hence, larger spatial scales. This assumption is no longer valid, so flow variation is introduced here. Simulations will be conducted with two flow distributions, representing the extreme cases. Both are instantaneously spatially uniform. In addition to modelling flow that is uniform in both space and time, flow whose direction of spatial uniformity varies in time will also be modelled. The angle of this flow will be distributed uniformly on $(0,2\pi)$. These flow conditions will be referred to as 'unidirectional' and 'varied' respectively.

It is assumed that the rate of change in direction of varied flow is effectively instantaneous and that there are prolonged periods where the flow is unidirectional. This means that individual uptake equilibrium is unaffected, but that large scale influences between clusters varies significantly. There is therefore no need to remodel the hydrodynamics. The rotational averaging is performed at an algebraic/numerical level, from the plankton concentration depletion field h, generated with unidirectional flow. A new field is obtained with numerical integration and linear interpolation, from the relationship

$$h_{\text{var}}(x,y,z) = \frac{1}{2\pi}\int_0^{2\pi} h(x\cos(\theta)+y\sin(\theta),-x\sin(\theta)+y\cos(\theta),z)d\theta \tag{49}$$

5.3 Benchmark Results

An intuitive starting point for simulations is to embed simple and even structures, to gauge an understanding of the dynamics at this scale of modelling and to provide a benchmark in the search for optimal arrangements. In keeping with the constraint of connectedness, rows and sheets of N mussels will be simulated, generating data for $Q(N)$ for both flow conditions. Simulations are performed for rows in unidirectional flow (Figures 17 and 18), sheets in unidirectional flow (Figures 19 and 20), rows in varied flow (Figures 21 and 22) and sheets in varied flow (Figures 23 and 24). Figures 17, 19, 21 and 23 show the mean of individual uptake rates, while Figures 18, 20, 22 and 24 show Q (the number of good quality mussels present), for each case.

5.4 Branching Model

In this Section, a model will be presented for generating arrangements for specific flow conditions. The model is designed such that, subject to certain assumptions, the generated arrangements will be optimal, according to the criteria given in Section 2.1. The primary assumption here is that the optimal configuration for N units contains the optimal configuration for N-1 units, so that the transition is made by simply adding one unit at an optimal location.

Diffusion Limited Aggregation (DLA) (Witten and Sander 1981) serves as inspiration for this approach. It involves the growth of a discrete structure one unit at a time, also DLA computer simulations are relatively simple to code. Traditional DLA are cellular automata models on a uniform grid, usually with a finite domain. 'Particles' are designated by occupied cells, which walk randomly around the domain. There is, initially, one fixed (seeding) particle in the centre. When other particles come into contact

with the fixed particle, they become fixed also, until all particles have settled, forming a fractal branching structure.

A variant of the traditional DLA will be used here, for two reasons. Firstly, the computer simulation for calculating uptake does not require that units must be located on a uniform grid. Secondly, a version that is simpler to code will allow more scope for introducing optimality considerations at each iteration. To replace the random walk process, an angle will be generated at random. A new particle will then be added, at that angle from the origin, at the extremity of the existing structure.

Coding this model for three dimensional branching growth requires uniformly distributed so-called 'solid' angles, which is equivalent to requiring points distributed randomly and uniformly on a sphere. For this, some statistical theory is given.

On a sphere, the increment of area is $dA = \sin(\phi)d\phi d\theta$, where θ and ϕ are the horizontal and vertical angles, respectively, in standard spherical polar co-ordinates. If ϕ and θ distributed by $p_1(\phi)$ and $p_2(\theta)$, the density on area dA will be

$$density(\phi,\theta) = \frac{p_1(\phi)p_2(\theta)d\phi d\theta}{dA} = \frac{p_1(\phi)p_2(\theta)}{\sin(\phi)} \tag{50}$$

If this density is to be constant with respect to ϕ and θ, p_1 must be some proportion of $\sin(\phi)$ and p_2 must be a constant. From their respective domains of definition, it is deduced that

$$\begin{aligned} p_1(\phi) &= 0.5\sin(\phi) \\ p_2(\theta) &= 1/2\pi \end{aligned} \tag{51a,b}$$

To generate random numbers from these distributions, r_1 and r_2, are taken from a uniform distribution between 0 and 1. The respective inverses of the cumulative functions are then applied, which are

$$p_1{}^C(\phi) = \int_0^{\phi} p_1(\lambda_1)d\lambda_1 = 0.5 - 0.5\cos(\phi)$$
$$p_2{}^C(\theta) = \int_0^{\theta} p_2(\lambda_2)d\lambda_2 = \theta / 2\pi \qquad (52a,b)$$

so that

$$\phi = \cos^{-1}(1 - 2r_1)$$
$$\theta = 2\pi r_2 \qquad (53a,b)$$

provide uniformly distributed points on a sphere.

As indicated, once a spherical angle has been generated, the N^{th} unit can be fixed onto the extremity of the N-1 unit structure, measured from the first unit at that angle. The size of the particles used to grow the branching structures have diameter 0.22 m, corresponding to the small scale domain length.

A branching structure was also generated for the two-dimensional case (Figure 25), where a unit in the horizontal plane represents a vertical rope, extending indefinitely. Figure 26 shows results for the growth of Q with respect to N, for this control case.

The simplest method of increasing the value of the objective function at each iteration is to select the best new placement from a finite set of options. That is, the arrangement of N units can be assessed k times, with the N^{th} unit in a different place each time. The arrangement yielding the best result is kept, which becomes the optimal configuration for N units.

Finding an appropriate value of k is a trade-off between computational speed and quality of the arrangement. In order to make this trade-off quantitative, the value of Q, for maximum N, will be predicted for various k, from the data obtained from the control case

Information on the effect of each introduced unit is available from the $Q(N)$ curve. In particular, the measure of success of each addition is reflected by the discrete derivative, dQ/dN. If β is defined by values of this derivative, then β has a negatively skewed distribution (Figure 27).

The $Q(N)$ curve can be considered as an accumulation of values taken from this distribution. Choosing the best of k options for the location of the N^{th} unit is equivalent to choosing the highest of k values taken from this distribution. The distribution of the highest of k values from the original distribution, is easily calculable.

Let $\beta = dQ/dN$ be distributed according to $f(\beta)$; $f^C(\beta)$ is the associated cumulative function. If $f^C(\beta)$ is the probability that a given value is less than β, the probability that k independent values are all less than β is $\left[f^C(\beta)\right]^k$. This is therefore the cumulative distribution $f_k{}^C(\beta)$, which merely requires differentiation, to give the improved probability density distribution, $f_k(\beta)$.

The predicted Q value is the sum of β, which is the product of N and the mean of β. That is,

$$Q(k) = N\sum[\beta\ f_k(\beta)]. \tag{54}$$

As seen in Figure 28, Q quickly approaches a supremum, so that there is decreasing benefit offered by increasing k. Based on this graph and on considerations of the required computational time to perform simulations, k is set at 10.

It is possible to predict the $Q_k(N)$ growth curve for k=10, from the cumulative frequency function $f_k{}^C(\beta)$. N values distributed uniformly between 0 and 1, filtered through the inverse of $f_k{}^C(\beta)$, form the derivative for the predicted curve. These are sorted to the same sequence as their equivalents from the $Q(N)$ curve for k=1, so that the same dynamics of temporal fluctuation and curvature are maintained. The resultant curve is compared with computational results, showing excellent agreement (Figure 29).

Two-dimensional branching structures for various flow conditions, number of mussels and spatial limitations are shown in Figures 30 to 37. First, structures in unidirectional flow with a 10 m square spatial limit are shown after growth to 135 units (Figure 30) and 270 units (Figure 31). Note that the number of mussels here are 8100 and 16200 respectively. Second, the spatial limit was reduced to 5 m, again structures are shown for 135 units (Figure 32) and 270 units (Figure 33), in unidirectional flow. For simulations in varied flow, circles were used as the spatial restriction as opposed to squares. Structures are shown for a 10 m diameter after 135 units (Figure 34) and 270 units (Figure 35). Lastly, structures are shown and for a 5 m diameter after 135 units (Figure 36) and full domain occupation (Figure 37), which occurred at 210 units.

Simulations for these branching structures have been performed with various spatial limitations; growth curves for $Q(N)$ were generated for unidirectional flow (Figure 38) and varied flow (Figure 39). For both flow conditions, spatial boundaries were set at 5 m to 10 m, with increments of 1 m. Imposing the 5 m boundary resulted in the lowest uptake for both conditions, ranging to the highest uptake for the 10 m case, which was to be expected.

Curves for unidirectional flow indicate distinct growth phases, followed by saturation periods, where Q is at its maximum. The maximal values for Q appear to be proportional to the imposed spatial limit. Results for the branching structures in varied flow are qualitatively different. Uptake reaches saturation point, then begins to decrease. There is not sufficient data to infer an explicit relationship between the maximal Q value and the spatial limit for this case.

Fractal Analysis

Describing these branching structures in terms of their fractal properties (e.g., Mandelbrot 1982, Kaandorp 1994) may aid in formulating grounds for comparison and, potentially, quantify the relationship between environment and growth structure (see Kaandorp 1999, Abraham 2001). In particular, their fractal dimension will be calculated. There are many methods for determining the fractal dimension of an object (e.g., Feder 1988, Kaye 1989, Falconer 1990, see also Hall and Wood 1993).

The first possibility is the 'Box Counting' method, which measures the object's 'mass' at various orders of resolution. Using a grid of resolution l, this is achieved by counting the number of grid boxes, B, which are occupied by the object. Plotting $\log(B)$ against $\log(l)$, the fractal dimension D_f can be found from the slope of the graph. This is deduced from the theoretical relationship

$$B = \alpha_B (l)^{-D_f} \tag{55}$$

where α_B is some constant coefficient.

This method relies on the self-similar nature of fractal objects and so requires that l ranges over a few orders of that self-similarity. Images from simulations, however, do not show sufficient orders of self-similarity and do not generate enough data points from which to accurately ascertain the slope of $\log(B)$ against $\log(l)$.

A second method for calculating the fractal dimension is to deduce D_f from the relationship

$$N = \alpha_N r^{D_f} \tag{56}$$

where N is the number of units within a radius, r, from the first unit; α_N is another constant coefficient. Using methodology similar to the Box Counting technique, D_f can be found from the slope of the graph of $\log(N)$ against $\log(r)$. Results are given in Table 3.

Table 3: Fractal Dimension for Branching Structures

Dimensionality	k value	Flow Conditions	D_f
3	1	Not incorporated	2.37
3	10	Unidirectional	2.05
3	10	Varied	2.08
2	1	Not incorporated	1.73
2	10	Unidirectional	1.61
2	10	Varied	1.51

The fractal dimensions of traditional DLA structures are known to be approximately 2.43 in three dimensions and 1.70 in two dimensions (e.g., Falconer 1990). Results here, for simulations not incorporating flow conditions, show reasonable agreement with these established values, despite a slightly different model being used and only a relatively small data set from which to calculate D_f.

In both two and three-dimensional simulation, the fractal dimension value D_f is measured to be significantly lower when $k = 10$. This is due to the adaptation of the structures to the flow condition, thus demonstrating preference for some dimensions over others.

It is observed is that D_f is lowest for unidirectional flow in three dimensions, but is lowest for varied flow in two dimensions. The three dimensional result is due to the fact that structures in unidirectional flow are mostly restricted to the two dimensions perpendicular to the flow. In two-dimensions, although structures in varied flow extend equivalently over both dimensions, the shape of the generated object is composed largely of linear sections.

5.5 Designed Structures

In this section, structures will be presented that have been explicitly designed to be potentially optimal. Concepts and trends from earlier results from Sections 5.3 and 5.4 assist intuition in arriving at these geometries.

Results from Section 5.3 indicate that arrangements spread perpendicular to the direction of unidirectional flow are significantly more efficient than those parallel to it. This concept of transversality extends to the three-dimensional analogue, a plane of mussels perpendicular to the flow. For values of N that can be divided evenly by the number filling the side of the domain cube, a series of planes is therefore suggested as the design for unidirectional flow. These planes will be adjacent, due to the requirement of connectedness.

Vertical columns are again the natural basic structure, in designing a configuration for varied flow. The layout of these columns in horizontal space is therefore the defining issue. Clearly, the more spread out the arrangement, the less the depletive effect and the higher the collective uptake. The issue thus becomes how to maximally spread out a connected structure within a limited domain. A spiral is suggested, since no unit is connected to more than its two adjacent units and it can be stretched to extend to the limiting boundary. Figure 40 shows the plan view of the designed configuration for varied flow.

5.6 Comparative Results

This section summarises the uptake efficiency results that have been obtained for various structures. To gauge the adaptability of the branching model to the flow, simulations were performed to assess each structure in the alternative flow condition to that in which

it was generated. That is, the arrangement generated in varied flow is tested in unidirectional flow and vice versa. Similarly, results are given for designed structures in both flow conditions. The inclusion of these extra data will indicate not only the optimal structure for each condition, but the sensitivity of uptake to the arrangement for each flow.

Tables 4 and 5 show results for structures in unidirectional flow with 5 m and 10 m boundaries respectively. Tables 6 and 7 show results for structures in varied flow, also with boundaries of 5 m and 10 m respectively. In Tables 4 to 7, 'Br' denotes branching, while 'Des' means designed. The parenthesised 'uni' or 'var' indicate the flow conditions in which that structure was generated or designed. Collective uptake is measured by Q, the number of good quality mussels present.

Table 4: Uptake in Unidirectional Flow with 5 m boundary

Units	45	90	135	180	225	270
Mussels	2700	5400	8100	10800	13500	16200
Br (uni)	2444	4623	4786	4720	4698	4695
Br (var)	2089	3694	4639	4458	4589	-
Des (uni)	2429	4542	4686	4674	4665	4665
Des (var)	1661	3155	4114	4394	4323	4653

Results here show that branching structures are optimal under conditions of unidirectional flow, but that sheets of mussels perpendicular to the flow are also highly efficient over the specified range of N values. It is also observed that efficiencies are increasingly similar between structures as N increases, as saturation is reached.

Table 5: Uptake in Unidirectional Flow with 10m boundary

Units	45	90	135	180	225	270
Mussels	2700	5400	8100	10800	13500	16200
Br (uni)	2444	4902	7265	8864	9124	9191
Br (var)	2089	3694	4892	6752	7740	8132
Des (uni)	2522	4914	7358	9331	9437	9406
Des (var)	2516	2967	5309	5503	7431	7505

The optimal arrangement, in scenarios with spatial domain increased to 10 m, is a sheet of mussels perpendicular to the flow, as is shown here in Table 5. Again, this result is persistent over the full range of N values.

Table 6: Uptake in Varied Flow with 5 m boundary

Units	45	90	135	180	225	270
Mussels	2700	5400	8100	10800	13500	16200
Br (uni)	2385	4789	6682	7148	6568	5929
Br (var)	2414	4817	7218	9355	10211	-
Des (uni)	2344	4480	3414	2283	1529	1108
Des (var)	2428	4852	7252	9507	10987	6113

Uptake efficiencies in varied flow appear to be more similar, for small N, than they are in unidirectional flow. At large N, however, the differences are increasingly apparent, showing spirals to be optimal under this condition, with slightly higher uptake than the branching structure.

Table 7: Uptake in Varied Flow with 10 m boundary

Units	45	90	135	180	225	270
Mussels	2700	5400	8100	10800	13500	16200
Br (uni)	2385	4793	7195	9347	10863	10908
Br (var)	2414	4817	7287	9648	12069	14446
Des (uni)	2406	4811	7088	8185	5841	3781
Des (var)	2434	4860	7312	9723	12109	14517

Results here are similar to the 5 m boundary case for varied flow, showing spirals to be the optimal arrangement. The branching structure performs also well in this condition.

It appears that the optimal arrangements identified here are dependent on the flow condition and on the scale of limitation, not on the number of mussels present. Criteria A (Page 9), which define optimal structures for each value of N, are therefore irrelevant here. Further, if the optimal structure is independent of the number of mussels, N can always be chosen such that Q/N is greater than the quality parameter p, for $p \leq 0.9$. Criteria B (Page 10) are therefore also redundant, making all sets of criteria equivalent definitions of optimality, for interpretation of these results.

These results provide framework for determining the optimal arrangement of mussels at this scale of consideration. However, it is likely that realistic flows will not be unidirectional or varied, but some combination thereof. It is therefore important to address how potentially optimal structures perform under a range of conditions. In particular, although sheets of mussels are optimal in unidirectional flow with a 10 m boundary, that arrangement performs poorly in varied flow. Secondly, although branching structures generated for varied flow are not optimal under any particular flow, they perform well in all conditions.

It may be that some combination of these structures is sought, that will capture the advantages of each. This is easily incorporated into the branching model. A specific flow condition can be implemented numerically, in the generation of the plankton depletion field (Equation 49). This approach will be discussed further in Chapter 6, in which the assimilation of hydrodynamic data into optimality considerations at the large scale will be discussed.

5.7 Unconnected Arrangements

It may be of interest to assess the efficiency of unconnected arrangements, in cases where practicality permits such a structure in the field. Although such configurations are ruled out from general optimality under all sets of criteria, a brief description is given here of one particular approach to addressing this issue. Representative results are also shown.

An intuitive initial arrangement, for a 10 m grid, is one in which all units of mussels are equally spaced in the square. This raises geometric questions about how to evenly space N units, when N is not a square number. The analytic treatment of this problem can be complicated and depends on how one defines 'evenly spaced'. Furthermore, there is no guarantee that the evenly spaced configuration for N units is similar to the evenly spaced configuration for N-1 units. Instead of tackling these issues, another approach is suggested.

Let N be fixed at 270 units of mussels. Let ρ be the density of those units and let s be a dimensionless parameter, reflecting the constant spatial gradient of ρ, in the x direction. That is, the density, ρ, varies linearly with x (Figure 41), according to the equation:

$$\rho(x) = 1 + s(2x - 1). \tag{57}$$

For all non-zero s, an unique configuration for the N units will be obtained, from which the uptake efficiency for various s can be measured.

In order for the density to be approximately equivalent in each of the horizontal directions, there must be, on average, $\sqrt{270}$ units along each dimension. Since the number of units must be a natural number, the rounded square root of 270 is taken, which is 16. This value becomes the number of columns in the arrangement. These columns will be spread along the length of the domain non-evenly, to reflect the density gradient s. The units in any given column will be spread out evenly, but the number of units in each must also reflect the spatial gradient of density. The requirement therefore, is an algorithm that calculates the positions of the 16 columns and the number of units in each column, for a given s value, while keeping the total number of units at 270.

A set of x values, x_u, can be constructed that exhibit this density variation, by applying a particular function to 16 evenly spaced values, x_e. To find this function, the differential equation

$$\frac{dx_u}{dx_e} = \rho(x) \tag{58}$$

is solved with the boundary conditions $x_u = 0$ when $x_e = 0$, to give

$$x_e = x_u(1-s) + sx_u^{\,2} \tag{59}$$

and thus the positions of the 16 columns:

$$x_u = \frac{s-1+\sqrt{(1-s)^2+4sx_e}}{2s}. \tag{60}$$

Next, the number of units in each column is calculated. These must total 270; each is proportional to the density value at its x location. That is, a scalar, r, is required, such that

$$\sum \text{round}(r\rho(x_u)) = 270. \tag{61}$$

The search for r involves beginning with two initial values which yield sums either side of 270 and calculating the sum for the midpoint of those values, which then becomes the new high or low bound. This is repeated until any r is found for which the sum equals 270.

Unfortunately, r will not always exist, so that there is no proof for the general existence of r. However, the conditions can be known for which r may not exist.

A problem will arise if there are two $r\rho(x_u)$ values that are both $^1/_2$, modulo 1, since the sum would increase by a step of two, as that value of r is approached. This would imply that the ratio of the two $\rho(x_u)$ values would be rational.

Let x_1 and x_2 be such an pair of members of the original evenly spaced vector, with $x_1 < x_2$. Then,

$$\frac{\rho(x_u(x_1))}{\rho(x_u(x_2))} = \frac{\sqrt{(1-s)^2 + 4sx_1}}{\sqrt{(1-s)^2 + 4sx_2}} \tag{62}$$

is rational. It is known that x_1 and x_2 are rational, because they are found from evenly dividing up the unit interval by an integer. The numerator is only rational if x_1 completes the square by being 0 or 1. Similarly, x_2 must be 0 or 1 if the denominator is to be rational. And since $x_1 < x_2$, it follows that $x_1 = 0$ and $x_2 = 1$. This means that

$$\rho(x_u(x_1)) = 1 - s \tag{63}$$

and

$$\rho(x_u(x_2)) = 1 + s\,. \tag{64}$$

If the restriction is imposed that s must be a multiple of 0.1, then r must be a multiple of 5 for $r\rho(x_u(x_1))$ and $r\rho(x_u(x_1))$ to be $^1/_2$ modulo 1. And, since r is expected in the range 16 to 18 (considering the approximate means of 270/16 units per column and unit

density), this will probably not occur. A check can be performed for this in the computer algorithm by using $r = 15$ and $r = 20$ as the initial values. If the calculated sums are either side of 270, the algorithm can proceed, confident of the existence of r. This was always the case.

Once positions on the unit square for the 270 units have been located (Figure 42), these are simply scaled up to the full domain, 10 m in length, allowing half a unit (0.11 m) adjacent to the boundary. Results for the unconnected arrangements are shown in Figure 43, considering uniform flow and density varying with x. These results indicate a maximum at approximately $s = 0.6$.

A second method of density variation involves the absolute value of x, so that

$$\rho(x) = 1 - s + 2s|2x - 1|. \tag{65}$$

Results for simulations according to this method of variation also indicate a maximum at $s = 0.6$, as shown in Figure 43.

Fewer simulations were performed for conditions of varied flow, due to the trends of the results. They are shown in Figure 44, where density varies with x.

This demonstrates that evenly spaced arrangements are optimal under these conditions.

5.8 Perturbation Technique.

An arrangement of N units is not optimal if, when perturbed a small and random amount, a larger value of Q results. In this case, it would be beneficial to adopt the new arrangement. On the other hand, if a smaller value of Q resulted, it would be advantageous to reject it. A simple algorithm is therefore constructed that searches for more efficient arrangements. The algorithm requires an initial configuration and, by

perturbing it incrementally, converges on a configuration that is locally optimal. The algorithm for this is as follows:

1. Calculate $Q_0(S_0)$.
2. Perturb configuration S_0 to S_1, subject to constraints.
3. Calculate $Q_1(S_1)$.
4. If $Q_1 \geq Q_0$:

   S_1 becomes new S_0,

   Q_1 becomes new Q_0,

   $a = 0$,

   Go to (2).
5. $a = a+1$.
6. If $a < A$, go to (2).
7. S_0 is optimal.

Here, a is merely a counter, so that A consecutive failed perturbations are interpreted to mean that S_0 is optimal.

Perturbation can be performed a number of ways, depending on the physical constraints of the arrangement. This methodology has been applied to a connected chain of units, in the following way:

Let x, y and z be the coordinate vectors of the N units. If the units form a chain, they can be described by vectors ϕ and θ, where

$$x_i = 0.22\sum_{j=1}^{i}\sin(\phi_j)\cos(\theta_j)$$

$$y_i = 0.22\sum_{j=1}^{i}\sin(\phi_j)\sin(\theta_j) \qquad \text{(66a-c)}$$

$$z_i = 0.22\sum_{j=1}^{i}\cos(\phi_j)$$

The distance between consecutive units,

$$\begin{aligned}\text{dist} &= \sqrt{(x_i - x_{i-1})^2 + (y_i - y_{i-1})^2 + (z_i - z_{i-1})^2} \\ &= 0.22\sqrt{\sin^2(\phi_i)\cos^2(\theta_i) + \sin^2(\phi_i)\sin^2(\theta_i) + \cos^2(\phi_i)} \\ &= 0.22\sqrt{\sin^2(\phi_i) + \cos^2(\phi_i)} \\ &= 0.22, \end{aligned} \tag{67}$$

is independent of ϕ and θ. This means that ϕ and θ can be varied without affecting the connectedness of the chain. ϕ and θ are first perturbed by small random vectors ε_ϕ and ε_θ respectively, then the above formulae for x, y and z are applied.

The distribution of of ε_ϕ and ε_θ affect the rate at which the configuration S will approach optimality. For simplicity, it is assumed that ε_ϕ and ε_θ are distributed uniformly between $-\varepsilon$ and ε. Increasing ε increases the rate of approach to optimality. However, finer searching is possible with smaller ε. A multi-phase system is therefore adopted, whereby once a reaches A, ε is decreased by a factor of 10, then the algorithm is repeated.

The resultant structures are shown in Figure 45, for chains limited to 50 and 60 units in a 10 m square.

This line of methodology will not be pursued beyond this point, since the generated structures are obviously not globally optimal. It is apparent that the results are too sensitive to the details of the algorithm and initial conditions to represent the physical environment satisfactorily. However, some further notes relating to theoretical development of the model will be given.

Applying this perturbation approach to more complex structures is difficult. To simplify coding, branching structures may be considered as several connected chains. These chains may be optimised either separately, or simultaneously. If the latter, an extra routine checking that no two chains touch must be included. This scenario could either be implicitly prevented through careful design of the perturbation function, or more easily, rejected if it occurs.

If the number of units is large, there is considerable potential for problems in this approach. Apart from the problem of computational load, there are issues surrounding numerical convergence. The perturbation technique does not have any associated guarantees of convergence, since the number of variables can be extremely large and numerical difficulties can be magnified. The number of variables, however, can be reduced by adopting a multi-scale approach. Particular parts of the structure can be optimised at the unit level, then the relative locations of the parts can be found in a second phase of optimisation. These phases can be repeated, considering that each part may now be orientated differently, or be in a location with different plankton concentration.

5.9 Discussion

This chapter has outlined theory and methodology for simulating a range of structures at the medium scale and assessing their uptake efficiencies. A model for generating optimal structures has also been presented. Uptake results for these structures have been compared with structures designed on the basis of the efficiencies of basic shapes.

Optimality definitions given in Section 2.1 are equivalent when comparing arrangements at this scale, since results show the optimal structure to be independent of the number of mussels, for all flow conditions and spatial limits. In unidirectional flow, branching structures were shown to be optimal in small domains; sheets (or nets) of mussels

perpendicular to the flow were optimal in large domains. Spiral structures were consistently optimal in varied flow.

Branching structures were found to perform well across all conditions of flow and spatial constraint, despite the fact they are only optimal in one of the four cases. This model for generating arrangements can also be extended to accommodate arbitrary flow distributions. The fractal dimensions of the branching structures have been calculated, which agree with established results and demonstrate the quantitative effect the environment has on the optimal fractal structure.

This chapter also included sections on unconnected arrangements and a possible additional computational tool for improving arrangements. While these topics are secondary to the optimality results reported for this scale, they provide increased insight into the general computational modelling of optimal structures, so have been included.

Chapter 6 – LARGE SCALE SIMULATION

This chapter discusses the extension of optimisation theory, methodology and results to largest scale consideration, such as a bay, or other potential location for a mussel farm. There are many simplifying assumptions that must be made in such an extension, involving difficult issues that are beyond the scope of this thesis, such as complex large scale flow and phytoplankton ecology.

The assessment of the efficiency of existing structures will be presented first. It is accepted that the identification of optimal structures at this scale is highly sensitive to the environment, so a generic methodology for achieving optimisation will be given.

6.1 Existing Arrangements

In this section, the efficiency of one mussel arrangement, currently used in New Zealand, will be explicitly measured. These structures are of the form of curved ropes, hung between floating structures (Figure 46).

A significant proportion of the length of rope is not perpendicular to the flow. In fact, the lengths of hanging rope form catenary curves, that is,

$$z(x) = \frac{1}{a}\cosh(ax), \tag{68}$$

with

$$-h/2 \le x \le h/2 \tag{69}$$

where h is the structure width.

The arc length of this curve is found, analytically, to be

$$\frac{2}{a}\sinh\left(\frac{ah}{2}\right). \tag{70}$$

A first approximation to this is the truncation of the sinh expansion after the third order term,

$$L=\frac{2}{a}\left(\frac{ah}{2}+\frac{a^3h^3}{48}\right)=h+\frac{a^2h^3}{24} \tag{71}$$

from which an estimate for a is obtained by

$$a=\sqrt{\frac{24(L-h)}{h^3}}. \tag{72}$$

A more accurate value for a may be found numerically by the Newton-Raphson method, that is, successive iteration of the following map,

$$a\to a-\frac{f(a)}{f'(a)} \tag{73}$$

where

$$f(a)=\frac{2}{a}\sinh\left(\frac{ah}{2}\right)-L. \tag{74}$$

Alternatively, a may be improved by successive iteration of the map

$$a\to\frac{a^2L}{2\sinh\left(\frac{ah}{2}\right)}, \tag{75}$$

depending on the particular values of h and L, which affect convergence. Next, x_e is defined as an evenly spaced vector from

$$\frac{-1}{la}\sinh\left(\frac{ah}{2}\right) \text{ to } \frac{1}{la}\sinh\left(\frac{ah}{2}\right) \tag{76}$$

at increments of 1. The mapping

$$x = \frac{1}{a}\sinh^{-1}\left(lax_e\right) \tag{77}$$

is then applied. This vector, x, along with

$$z = \frac{1}{a}\cosh(ax) \tag{78}$$

provide the Cartesian co-ordinates of an approximate catenary curve, with width h, arc increments l and total length L. The structure is found by setting l = 0.22 m, also L = 3 m and 25 m for the shallow curve and the deep curve respectively. The width h is varied from 2 to 6 m. The computational model of the structure, for h = 6, is shown in Figure 47.

These structures are situated in unidirectional flow conditions. All the rope sections on the deep curve are perpendicular to the flow, so that the drag force they impose on the flow will be equal. However, this is not the case with the shallow section. It is known from the above that the slope of the curve is sinh(ax), so that the angle of orientation to the flow is

$$\theta = \pm\tan^{-1}\left(\sinh(ax)\right). \tag{79}$$

Treatment of oblique rope sections was documented in Section 4.4, in the context of simulation at the smallest scale. Forces exerted by the water, at a velocity of 0.05 m/s,

onto the clusters was calculated for rope at various angles in that chapter. A periodic function interpolating these data points was given, of the form:

$$F(\theta) = \sum_{i=0}^{4} c_i \cos(i\theta). \tag{80}$$

The calculations for the drag force indicated negligible asymmetry around $\theta = \pi/2$, so that only orientations over the range $0 \le \theta \le \pi/2$ are addressed.

In this way, the drag force can be directly calculated for each unit. Also, it is known that the drag force reduces with reduced velocity, according to

$$F(V) = F(V_{0.05})\left(\frac{V}{V_{0.05}}\right)^2, \tag{81}$$

since force increases with V^2, assuming the velocity does not vary outside the range that will affect the drag coefficient.

Since the force exerted by each unit is potentially different, the system cannot be simplified by applying the dynamical systems approach outlined in Section 5.1. All units will be implemented into the system and the resultant uptakes can be directly calculated. Simulating the entire mussel farm at the medium scale is too computer intensive. It is possible, however, to make use of the repeating nature of the structure. By considering the volume enclosing these repeating shapes as units for large scale simulation, the whole farm can be included within the simulation domain.

The repeating shape includes two drops of the deep curved rope and two of the shallow. This is encased in a volume of length and width 6m and a depth of approximately 12m. The length of rope in this macro-unit is 56 m, which, when divided into 0.22 m units,

generates 255 units. N is therefore 15300. Results for simulations at this scale are given in Table 8.

Table 8: Uptake for the Large Scale Macro-unit

Width (m)	Q	Q/N
2	8404	0.55
4	8436	0.55
6	8510	0.56

Simulation at the large scale involves computing the efficiency of a connected series of these units. Results are given for total farm lengths of 90 m and 180 m, that is, 15 and 30 units. N = 1377000 and 2754000 in these cases respectively.

Table 9: Uptake for Various Farm Lengths and Widths

Length (m)	Width (m)	Q	Q/N
90	2	636921	0.46
90	4	639815	0.46
90	6	641838	0.47
180	2	1077558	0.39
180	4	1116344	0.41
180	6	1144087	0.42

Results show minimal variation of uptake with differing widths, h. It is also seen that the general efficiency of this farm arrangement appears to be adequate, based on indications from optimality results at the medium scale. However, at this stage there are no other large scale structures with which these might be compared.

6.2 Practical Implementation

There is limited advantage in continuing the computation of general optimal structures into scales at the bay level. This is because environmental conditions such as hydrodynamics, tidal patterns and plankton ecology are unique to each location. A theoretically optimal structure should take into account these influences. A results orientated approach would therefore introduce numerous simplifications and assumptions.

It is more useful to address how large scale physical data can be assimilated into the optimisation methodology outlined in this thesis. This section presents an outline for application of the model to identifying optimal mussel farm structures in specific environments, which will be referred to as bays, for convenience.

The bay must be divided into zones, which will become the domains for medium scale simulation. A defining property of the medium scale is that the water flow is instantaneously uniform throughout the domain. Hydrodynamic data will indicate areas of circulation, which must be split into smaller zones, so that velocity within each zone is temporally, but not spatially, dependent. These zones need not be the same size and shape.

A second characteristic of the medium scale domain is that local plankton levels are assumed to be constant. If the plankton distribution is known to be highly non-homogeneous, this will necessitate further division into smaller zones.

Thirdly, there is a computational restriction on the number of mussel clusters within each zone. Present facilities limit the number of clusters to approximately 270. In the case of large zones, where this number could easily be exceeded, a further split is necessary. However, if the region of homogeneity is sufficiently large, zones need not be strictly defined within that region. Zoning could be left flexible within that region. In that case,

the results for a representative zone could be given, which would then be applied to any potential zone in that region of the same size and shape.

Ideally, the time distribution of flow direction within each zone can be quantified, along with the relative plankton concentrations. The flow distribution will be in the form of the 'unidirectional' or 'varied' flow, as described in Section 5.2. Further, if the flow is close enough to being either unidirectional or varied, no medium scale simulation is necessary; earlier results may be taken directly into the large scale.

Otherwise, the new direction distribution, expressed as $g(\theta)$, over $0 \leq \theta < 2\pi$, with

$$\int_{\theta=0}^{2\pi} g(\theta)d\theta = 1, \tag{82}$$

can be incorporated at the algebraic level. This is done by generalising Equation 49, from Section 5.2, to

$$h_g(x, y, z) = \int_0^{2\pi} g(\theta)h(x\cos(\theta) + y\sin(\theta), -x\sin(\theta) + y\cos(\theta), z)d\theta\,. \tag{83}$$

Simulations can then be performed using the branching model with this new plankton concentration field.

Uptake rates, computed for each zone, are incorporated into the large scale simulation phase, taking into account the scaling effect of local plankton levels for each zone.

Optimisation methodology at the large scale will depend primarily on the number of mussels within each zone, the number of desired occupied zones, the existence of multi-zone regions, as well as constraints such as connectedness and the total allowable number of mussels.

If each zone is specified outright, the zone may either be occupied or vacant in the larger arrangement. The combinations of occupied zones that are feasible will depend on the optimality constraints mentioned above. If there are multi-zone regions, where zones are not specified individually, some of the additional medium scale methodology may be useful at the large scale, in particular, the branching model.

Chapter 7 – SUMMARY

A new methodology has been presented for generating optimal mussel farm structures, according to efficiency definitions for phytoplankton uptake and optimality criteria.

The Lattice Boltzmann Method for hydrodynamic modelling was utilised, due to its ability to accommodate the complex geometry of mussel clusters. This model has been expanded to include plankton dynamics and filtration by individual mussels. Simulations were then performed at three distinct scales of consideration, at resolutions 0.004 m, 0.22 m and approximately 6 m respectively.

An attempt has been made to integrate the hierarchy of scales of modelling, but their implicit distinction has meant that many results are particular to a certain scale. This is to be expected from a multi-scale problem. To establish the required links, the approach has been to use results from each scale as parameters for the next.

At the first scale of modelling, quantities such as plankton diffusion and mussel density on a cluster were varied. It was found that diffusive conditions did not significantly affect the optimal arrangement, which was full configuration of 60 mussels in a 0.22 m cube. Simulations for various rope orientations were performed, to gauge the sensitivity of uptake and drag force on the angle of this full cluster to the flow. It was found that uptake is highest when the rope is perpendicular to the uniform flow, as is the force imposed on the local water volume. These results did not lead to non-trivial optimality solutions, but were useful in providing computational parameters for modelling existing structures at higher scales.

The medium scale of modelling saw the incorporation of more general flow conditions, which was made possible on an algebraic level. First, various benchmark results were given, in particular the efficiencies of rows and sheets of mussel units. A branching

model was presented that approximates optimal solutions for any set of flow conditions, which was applied to two representative extreme conditions, unidirectional and varied flow. Other structures that were intuitively designed were also simulated and compared with the results from the branching arrangements. The optimality of unconnected arrangements was also considered, along with the theoretical and algorithmic considerations surrounding that issue.

Large scale modelling involved direct assessment of current structures, that is, existing mussel farms in New Zealand. Results were indicative of satisfactory arrangements, but were not compared with optimal efficiencies at that scale. Instead, methodology was presented for implementing the multi-scale optimisation for an environment such as a bay. Measured hydrodynamic data can be assimilated into the model at the medium scale, in what have been defined as medium scale homogeneous *zones* of the larger domain.

Overall research has relied on various limiting assumptions in order to simplify analysis and to reduce the optimisation task. These simplifications have included the linear relationship between plankton concentration and uptake by filtration, the hydrodynamic independence of mussel clusters at the medium scale of modelling, the constancy of ambient flow speed and the characterisation of flow conditions as unidirectional and varied.

Incorporation of the full functional response curve would bring a higher level of complexity into efficiency calculations and make the transition from small scale to medium or large scale modelling extremely difficult. It is unlikely that this would lead to different results for optimal structures, but such consideration would be a possible topic for further research.

Similarly, rejecting the assumption that mussel clusters are hydrodynamically independent at the medium scale would generate difficulties when incorporating the flow into simulations at that scale. This is because the local flow distribution would then be dependent on the ensemble arrangement of cluster units, as well as the overall flow

characteristics. Optimisation methodology would then require extensive flow modelling for each potential arrangement, making any iterative technique computationally intensive. Moreover, problems with scale transition would arise, since large scale arrangements would affect medium scale hydrodynamics, affecting what is optimal at the medium scale.

At all scales, flow velocity has been varied in direction only, leaving flow speed constant. This is possibly the most unrealistic simplification. However, it is noted that mussels grow significantly over their lifetime. Assuming the constancy of mussel shape, performing simulations for small mussels would simply reduce the modelling scale, in particular the Reynolds and Péclet numbers, which are equivalently restored by increasing ambient velocity. That is, modelling large mussels at low velocities is equivalent to modelling small mussels at high velocities, so that the optimal structure remains constant.

The assumption that flow can be characterised as unidirectional or varied was discarded in Section 6.2, in which arbitrary flow distributions were addressed in order to generalise the applicability of the optimisation methodology. However, the assumption of periods of flow uniformity was retained. This raises possibilities for further research at the small scale of consideration, of how plankton dynamics and optimal configurations are affected by dynamic flow variation. There is also the question of how the results from this research would be incorporated into multi-scale optimisation.

The practical implementation of the overall methodology leads naturally into the possibility of applying these documented results and algorithms to a case study of a potential farm site. It is not known how well realistic hydrodynamic and ecological data would suit the model and assumptions used in this research. Such a study would therefore not only lead to generating mussel farm structures that are theoretically optimal for specific sites, but also aid in improving this optimisation methodology to accommodate the physical environment more realistically.

Although this study has involved mussel farms, there is also potential for its application to other questions of optimisation in the physical sciences, in particular, topics involving complex geometry. For example, this approach may lead to increased understanding of the mechanisms behind, also the reasons for, the fractal complexity in nature.

Lastly, the aspects of this study not relating to optimisation, that is, the extension of Lattice Boltzmann modelling to incorporate other biophysical elements, would provide a fruitful area for further research. Hydrodynamic and ecological models have both progressed greatly, but their combination remains in relative infancy. This is largely due to the interdisciplinary nature of such modelling tasks and to the inherent differences in respective scales of modelling.

REFERENCES

Abraham E.R. (2001) The fractal branching of an arborescent sponge. *Mar. Bio.* 138: 503-510.

Barker C., Jorgensen (1996) Bivalve filter feeding revisited. *Mar. Ecol. Prog. Ser.* 142: 287-302.

Benzi R., Succi S., Vergassola M. (1992) The lattice Boltzmann equation: theory and applications. *Phys. Rept.* 222: 145-197

Best B.A. (1988) Passive suspension feeding in a sea pen: Effects of ambient flow on volume flow rate and filtering efficiency. *Bio. Bull.* 175: 332-342.

Boghosian B.M., Yepez J., Alexander F.J., Margolus N.H. (1997) Integer lattice gases. *Phys. Rev. E* 55: 4137-4147.

Bushnell D.M., Moore K.J. (1991) Drag reduction in nature. *Ann. Rev. Fluid Mech.* 23: 65-79.

Chen S., Doolen G.D. (1998) Lattice Boltzmann method for fluid flows. *Ann. Rev. Fluid Mech.* 30: 329-364.

Denman K.L., Gargett A.E. (1995) Biological-Physical Interactions in the Upper Ocean: the role of vertical and small scale transport processes. *Ann. Rev. Fluid Mech.* 27: 225-255.

Faber T.E. (1995) *Fluid Dynamics for Physicists*. Cambridge Uni. Press.

Falconer K. (1990) *Fractal Geometry. Mathematical Foundations and Applications*. John Wiley.

Feder J. (1988) *Fractals*. Plenum, N.Y.

Ferziger J.H., Peric M. (1999) *Computational methods for fluid dynamics*. Springer-Verlag NY Inc.

Frechette M., Butman C.A., Geyer W.R. (1989) The importance of boundary-layer flows in supplying phytoplankton to the benthic suspension feeder, *Mytilus edulis L. Limnol. and Oceanog.* 34(1):19-36.

Filippova O., Hanel D. (1997) Lattice Boltzmann Simulation of Gas-Particle Flow in Filters. *Computers and Fluids* 26: 697-712.

Frisch U., Hasslacher B., Pomeau Y. (1986) Lattice-Gas Automata for the Navier-Stokes Equation. *Phys. Rev. Lett.* 56: 1505-1508.

Galdi G.P. (1994) *Progress in theoretical and computational fluid mechanics*. Harlow Longman Scientific and Technical.

Gardner M. (1970) The Fantastic Combinations of John Conway's New Solitaire Game 'Life'. *Sc. Am.* 223: 120-123.

Giraud L., Popinet S. (1994) *Simulation numérique d'écoulements complexes par la méthode de Boltzmann sur réseau*. Projet de fin d'études ENSAM.

Grant J., Bacher C. (2001) A numerical model of flow modification induced by suspended aquaculture in a Chinese bay. *Can. J. Fish. Aquat. Sci.* 58: 1003-1011.

Hall P., Wood A. (1993) On the performance of box-counting estimators of fractal dimension. *Biometrika* 80 (1): 246-252.

Hou S., Zou Q., Chen S., Doolen G.D., Cogley A.C. (1995) Simulation of Cavity Flow by the Lattice Boltzmann Equation. *J Comp. Phys.* 118: 329-347.

Hurd C.L., Harrison P.J., Druehl L.D. (1996) Effect of seawater velocity on inorganic nitrogen uptake by morphologically distinct forms of *Macrocystis integrifolia* from wave-sheltered and exposed sites. *Mar. Bio.* 126 (2): 205-214.

Kaandorp J.A. (1994) *Fractal Modelling: Growth and Form in Biology*. Springer-Verlag N.Y. Inc.

Kaandorp J.A. (1999) Morphological analysis of growth forms of branching marine sessile organisms along environmental gradients. Mar Bio 134: 295-306.

Kandhai D., Vidal D.J.-E., Hoekstra A.G., Hoefsloot H., Iedema P., Sloot, P.M.A. (1998) A Comparison between Lattice-Boltzmann and Finite-Element Simulations of Fluid Flow in Static Mixer Reactors. *Int. J. Mod. Phys. C.* 9 (8): 1123-1128.

Kaye B.H. (1989) *A random walk through fractal dimensions*. V.C.H.

Lehman J.T., Botkin D.B., Likens G.E. (1975) The assumptions and rationales of a computer model of phytoplankton population dynamics. *Limnol. Oceanogr.* 20: 343-364.

Mandelbrot B.B. (1982) *The fractal geometry of nature*. Freeman, N.Y.

Martys N.S. (2001) A Classical Kinetic Theory Approach to Lattice Boltzmann Simulation. *Int J. Mod. Phys.* 12: 1169-1178.

Masselot A., Chopard B. (1998) A Multiparticle Lattice-Gas Model for Hydrodynamics. *Int. J. Mod. Phys. C* 9: 1221-1230.

Meyhofer E. (1985) Comparative pumping rates in suspension-feeding bivalves. *Mar. Bio.* 85: 137-142.

Monin A.S., Yaglom A.M. (1975) *Statistical Fluid Mechanics: Mechanics of Turbulence, Vol. 2*. M.I.T. Press.

Nikora V., Green M., Thrush S., Hume T., Goring D. (2002a) Structure of the internal boundary layer over a patch of horse mussels (*Atrina zelandica*) in an estuary. *Journal of Marine Research* 60(1): 121-150.

Nikora V., Goring D., Biggs B. (2002b) Some observations of the effects of micro-organisms growing on the bed of an open channel on the turbulence properties. *J. Fluid Mech.* 450: 317-341.

Nikora V., Goring D., Ross A. (2002c) The structure and dynamics of the thin near-bed layer in a complex marine environment: a case study in Beatrix Bay, New Zealand. *Estuarine, Coastal and Shelf Science* 54(5): 915-926.

Oreskes N., Shrader-Frechette K., Belitz K. (1994) Verification, validation and confirmation of numerical models in the earth sciences. *Science* 263: 641-646.

Pilditch C.A., Grant J., Bryan K.R. (2001) Seston supply to sea scallops *(Placopecton magellanicus)* in suspended culture. *Can. J. Fish. Aquat. Sci.* 58: 241-253.

Redhead M. (1980) Models in Physics. *British Journal for Phil. of Sci.* 31:145-163.

Ren J.S., Ross A.H. (2001) A dynamic energy budget model of the Pacific oyster *Crassostrea gigas*. *Ecological Modelling* 142(1-2): 105-120.

Riisgard H.U., Mohlenberg F. (1979) An improved Automatic Recording Apparatus for Determining the Filtration Rate of *Mytilus edulis* as a function of Size and Algal Concentration. *Mar. Bio.* 52: 61-67.

Ross A.H., Nisbet R.M. (1991) A dynamic model of growth and reproduction of the mussel *Mytilus edulis L. Functional Ecology* 4: 777:787.

Ross A.H., Gurney W.S.C., Heath M.J. (1994) Comparative dynamics of four fjord ecosystems. *Limnol. & Oceanogr.* 39(2): 318-343.

Rothman D., Zaleski S. (1997) *Lattice-Gas Cellular Automata: Simple Models of Complex Hydrodynamics*. Cambridge Uni. Press.

Russel-Hunter W.D. (1970) *Aquatic Productivity - an introduction to some basic aspects of biological oceanography and limnology*. Collier-MacMillan Canada Ltd.

Stacey M.T., Cowin E.A., Powell T.M., Dobbins E., Monismith S.G., Koseff J.R. (2000) Plume dispersion in a stratified, near-coastal flow: measurement and modelling. *Continental Shelf Res.* 20: 637-663.

Stevens C.L. (2003) Turbulence in an estuarine embayment: Observations from Beatrix Bay, New Zealand. *J. Geophys. Res.* 108 (C2): 2003-2017.

Succi S., Benzi R., Higera F. (1991) The L.B.E.: a New Tool for Computational Fluid Dynamics. *Physica* D 47: 219-230.

Taub A.H., editor (1963) *John von Neumann Collected Works*. The MacMillan Co., NY.

Toffoli T., Margolus N. (1987) *Cellular Automata Machines: a new environment for modelling*. Massachusetts Institute of Technology Press.

Tritton D.J. (1998) *Physical Fluid Dynamics* (2nd Edition). Oxford Uni. Press.

Tutar M. (2001) Computational modelling of flow around a cylinder in sub-critical flow regime with various turbulence models. *Int. J. Numerical Methods in Fluids* 35: 763-784.

Valiela I. (1995) *Marine Ecological Processes*. Springer-Verlag N.Y. Inc.

Vogel S. (1994) *Life in Moving Fluids: the physical biology of flow*. Princeton Uni. Press.

Witten T.A., Sander L.M. (1981) Diffusion-Limited Aggregation, a kinetic critical phenomenon. *Phys. Rev. Lett.* 47: 1400-1403.

Wolfram S. (1986) Cellular Automaton Fluids 1. Basic Theory. *J. Stat. Phys.* 45: 471-526.

Wolfram S. (1994) *On Cellular Automata and Complexity*. Addison-Wesley Publication Co.

Xi H., Peng G., Chou S. (1999) Finite-volume lattice Boltzmann schemes in two and three dimensions. *Phys. Rev. E* 60: 3380-3388.

LIST OF TABLES

LIST OF FIGURES

FIGURES

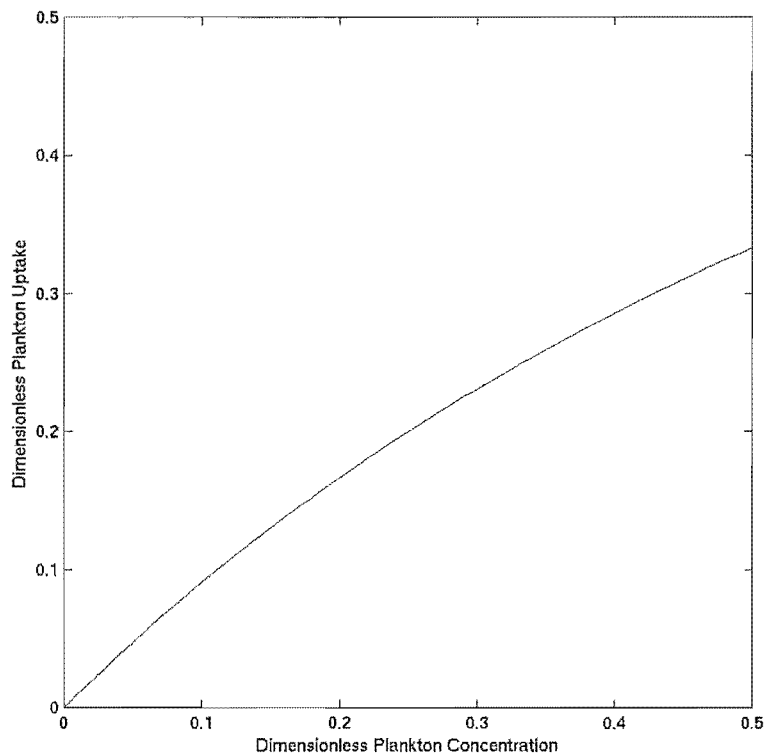

Figure 1. Functional response curve indicating uptake efficiency for varying local plankton concentration.

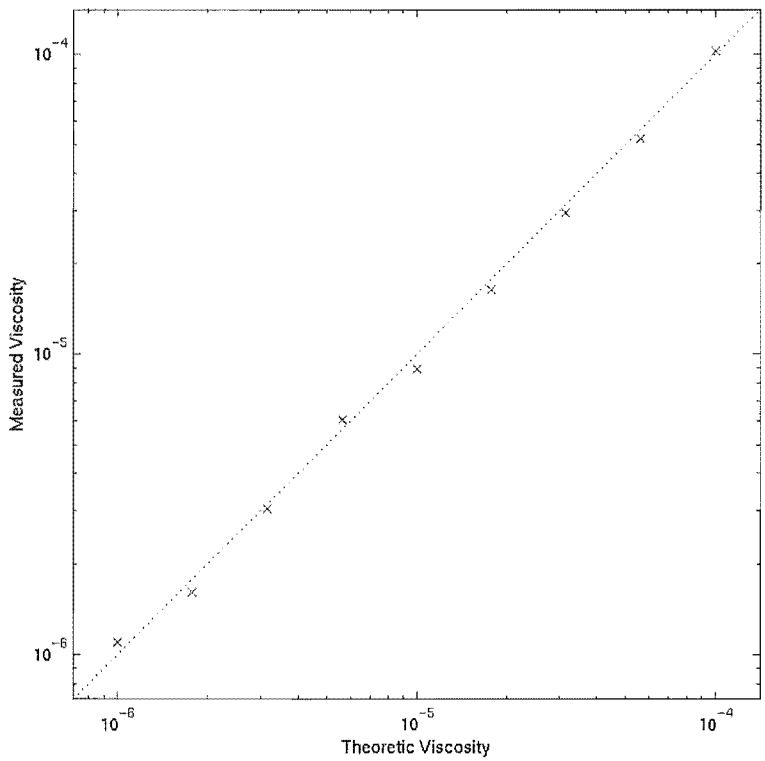

Figure 2. Comparison between theoretic and measured viscosity (m^2/s).

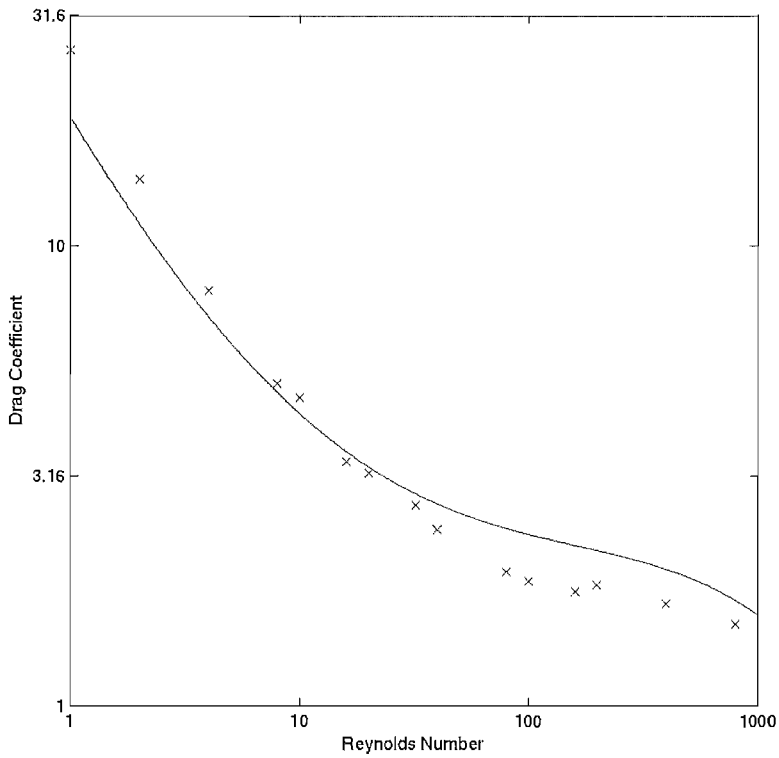

Figure 3. Drag Coefficient vs. Reynolds number for flow past a cylinder. The solid line is the known empirical relationship and the crosses are the measured data from force calculations.

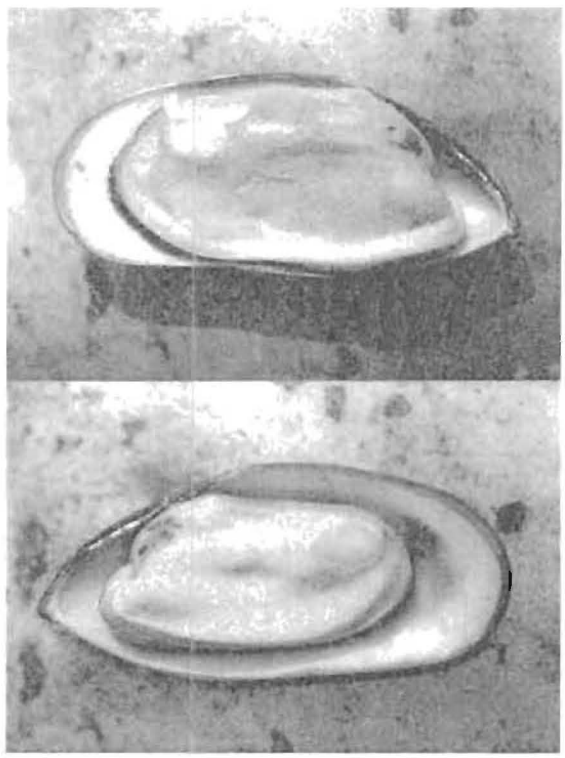

Figure 4. Male and female mussels. These digital photographs were utilised for the reproducing the exterior geometry of a mussel in the model.

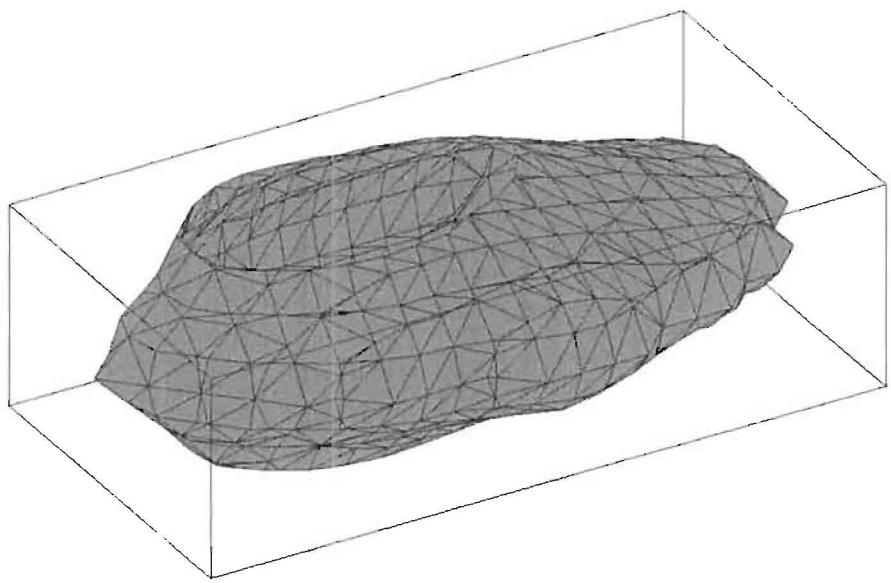

Figure 5. Digital three-dimensional model of an individual mussel.

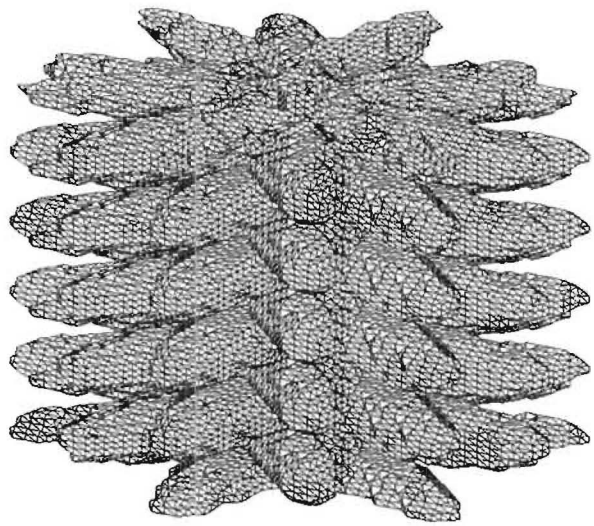

Figure 6. Cluster of 60 mussels, after incorporation into the LB Model.

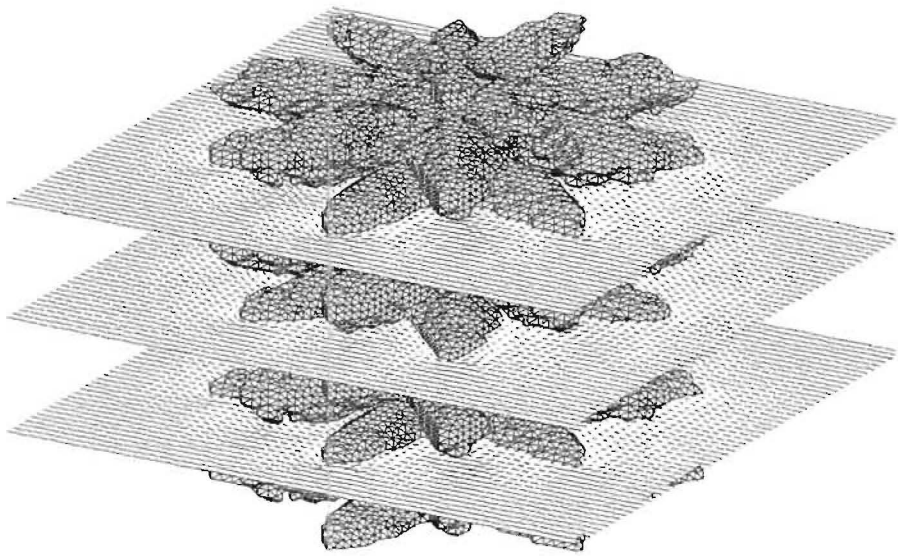

Figure 7. Horizontal sections showing water velocity field.
Flow is from upper left to lower right, with an upstream velocity of 0.05 m/s.

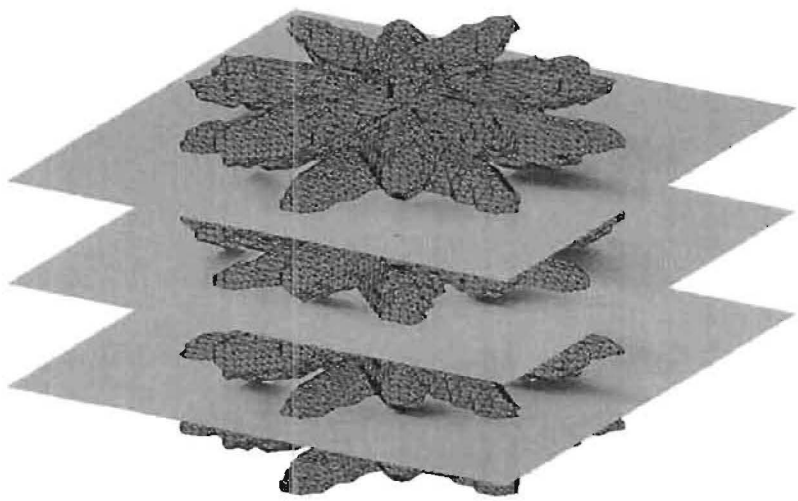

Figure 8. Horizontal sections showing plankton distribution.
Flow is from upper left to lower right.
Zones of plankton depletion are indicated by the darker areas.

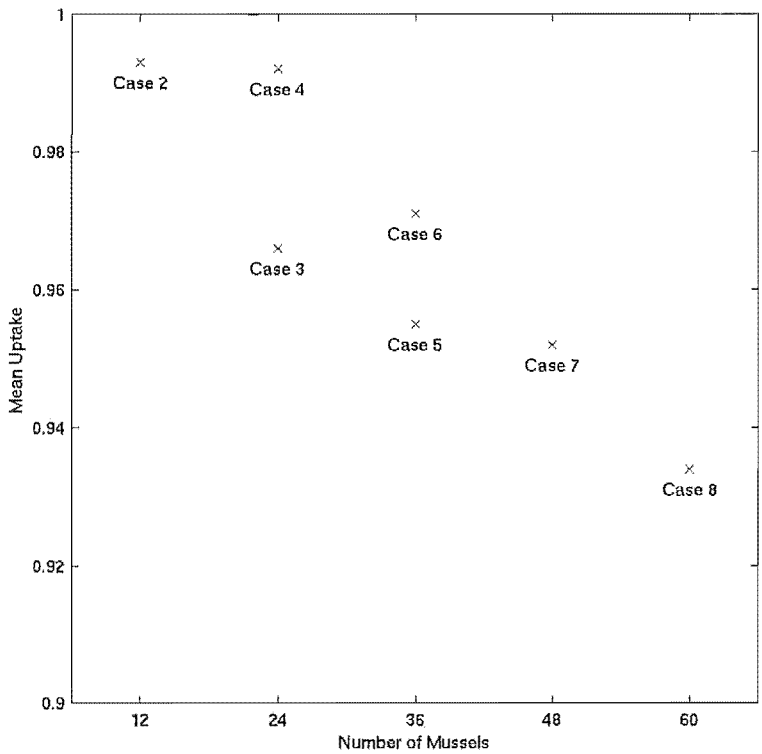

Figure 9. Mean plankton uptake for various mussel densities within a cluster.

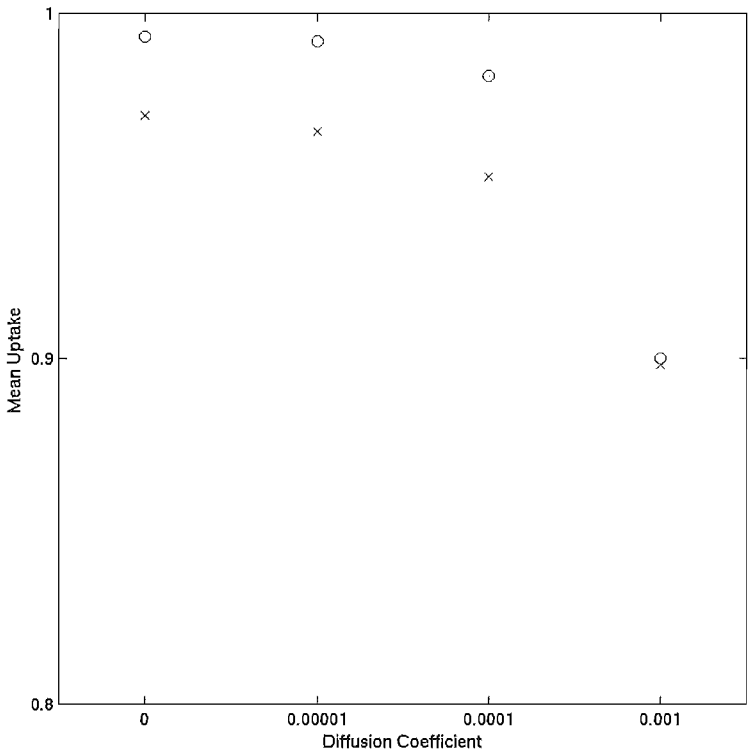

Figure 10. Mean plankton uptake with varying diffusion coefficient (m^2/s). Simulations were performed with 2 layers (24 mussels), where the layers were adjacent (crosses) and non-adjacent (circles).

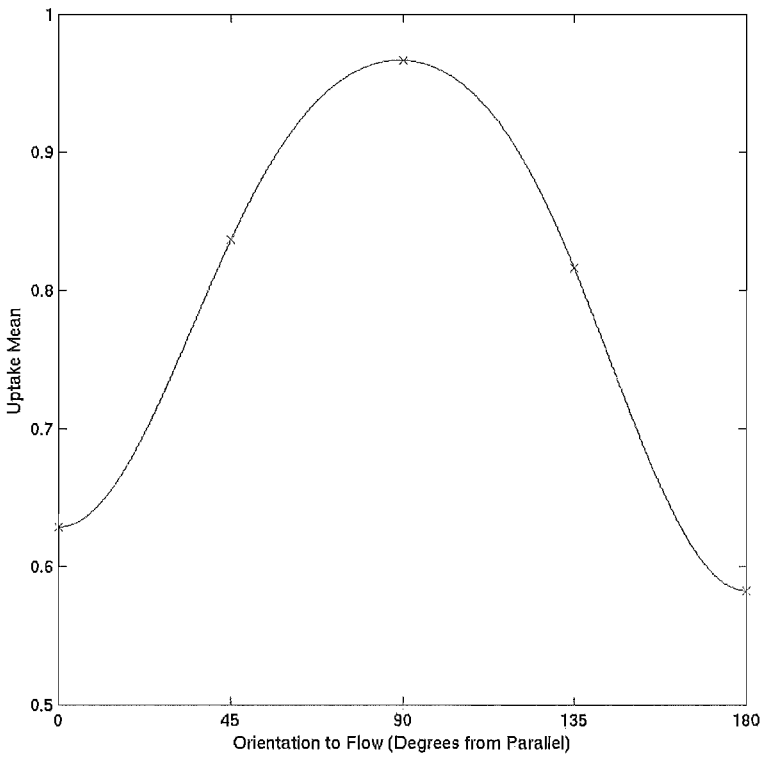

Figure 11. Mean plankton uptake with varying orientation of the rope to the water flow.

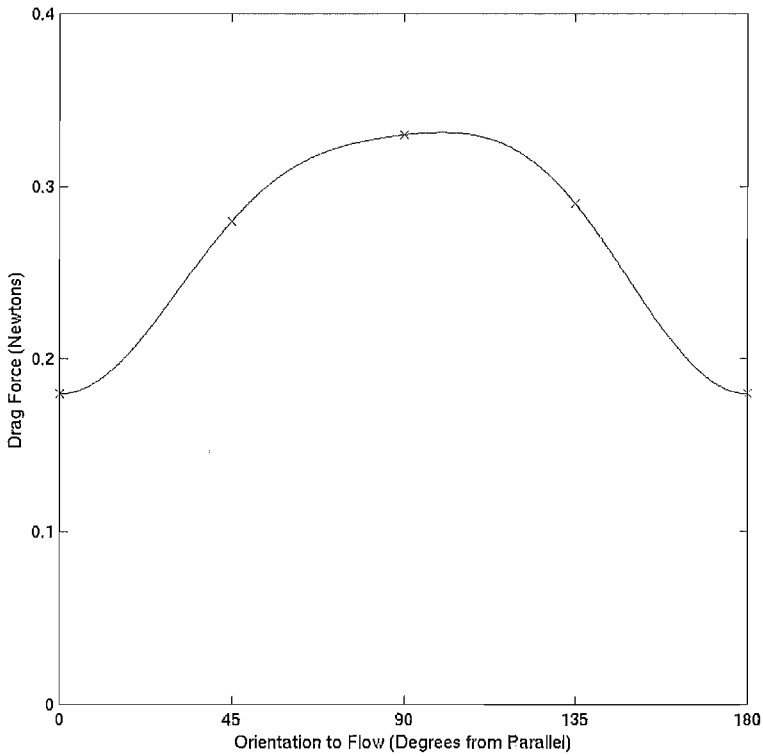

Figure 12. Drag Force with varying orientation of the rope to the flow.

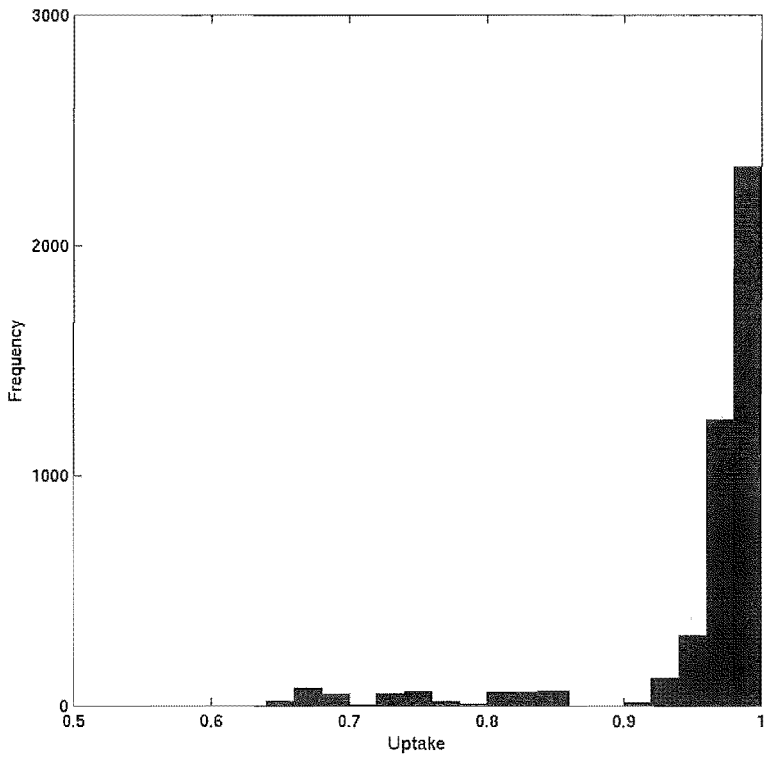

Figure 13. Distribution of individual uptake rates.

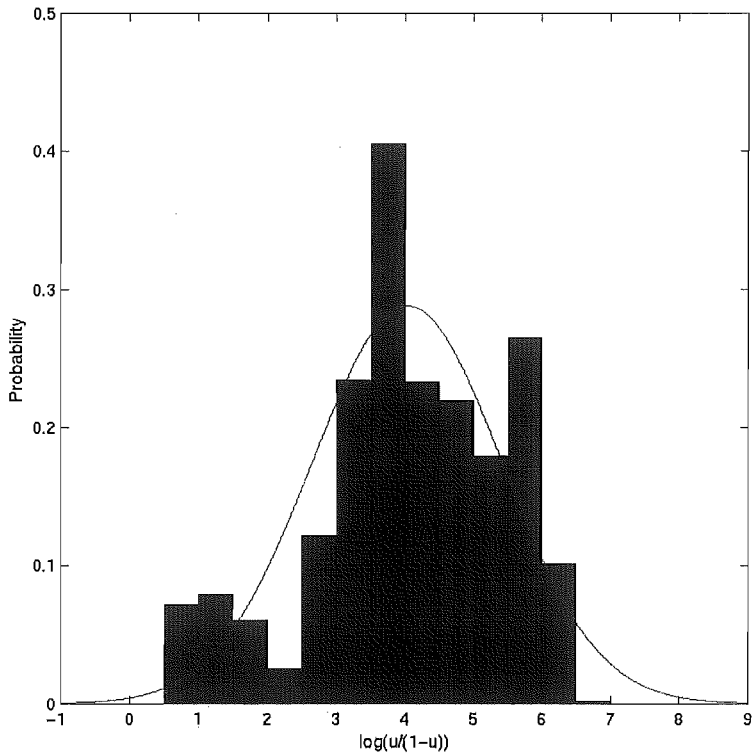

Figure 14. Distribution of mapped uptake rates (histogram) and generated normal curve (thin line).

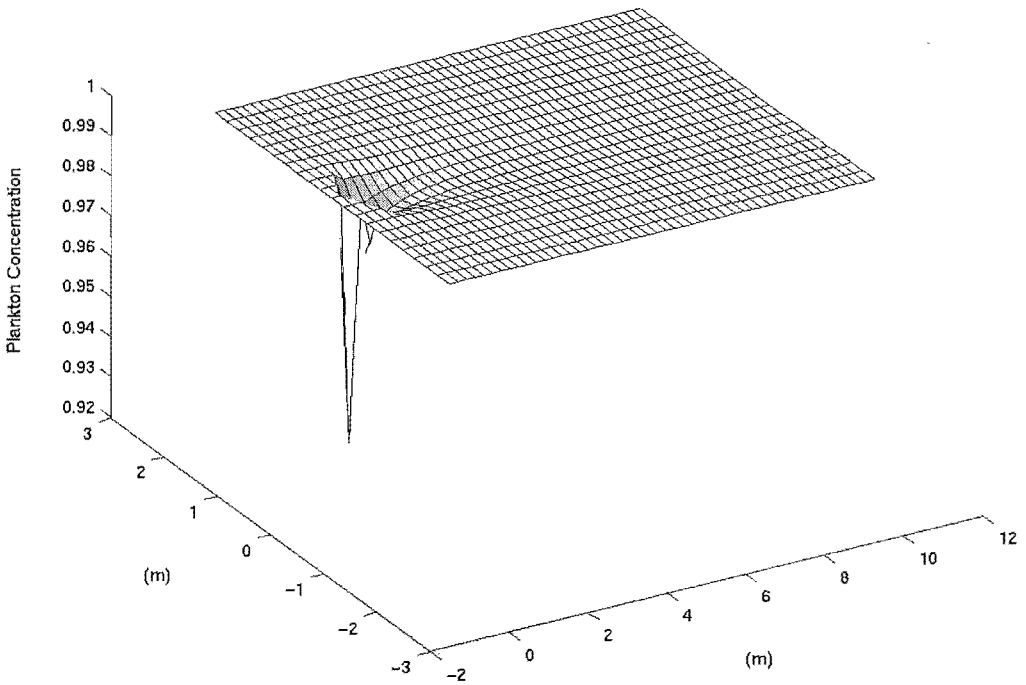

Figure 15. Plankton concentration field generated by a single unit of mussels at the origin. The dark area indicates plankton depletion.

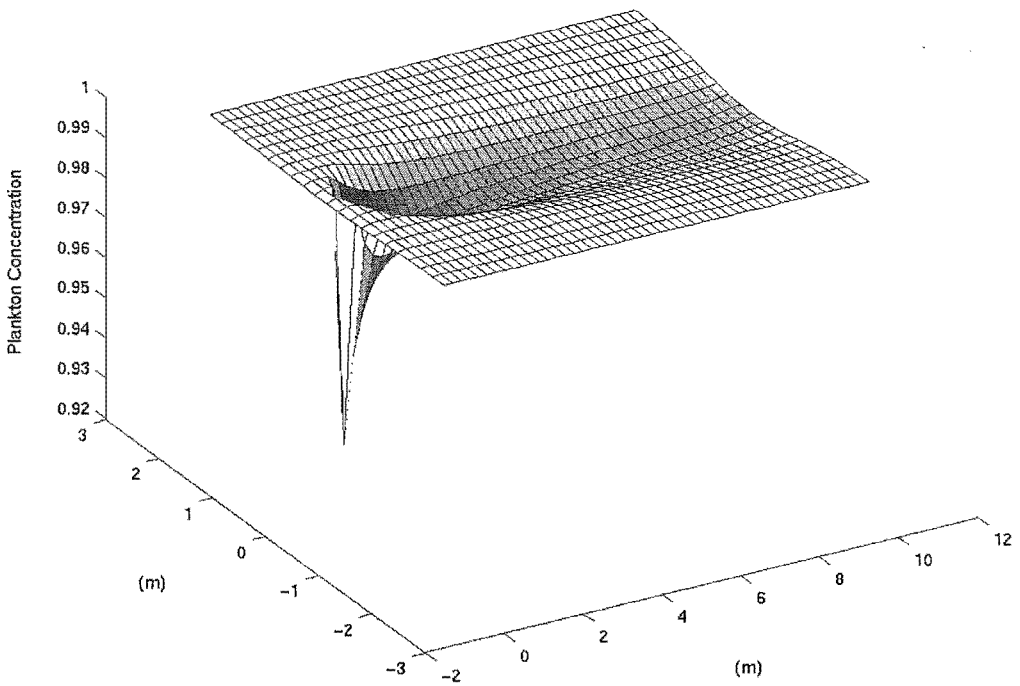

Figure 16. Plankton concentration field generated by a vertical column of units of mussels through the origin. The dark area indicates plankton depletion.

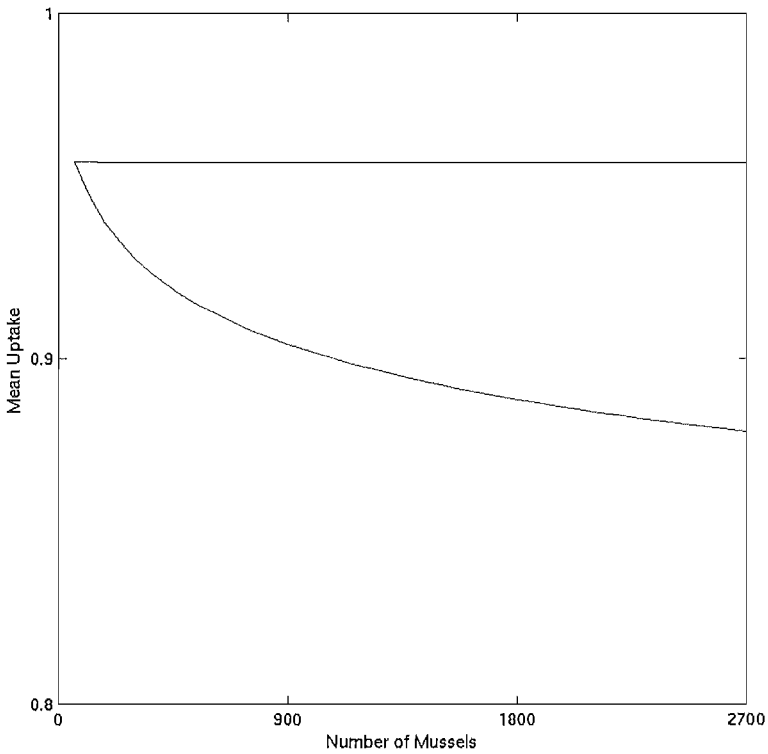

Figure 17. Efficiency of rows of units in unidirectional flow. The upper curve is a row perpendicular to the flow and the lower curve is a row parallel to the flow.

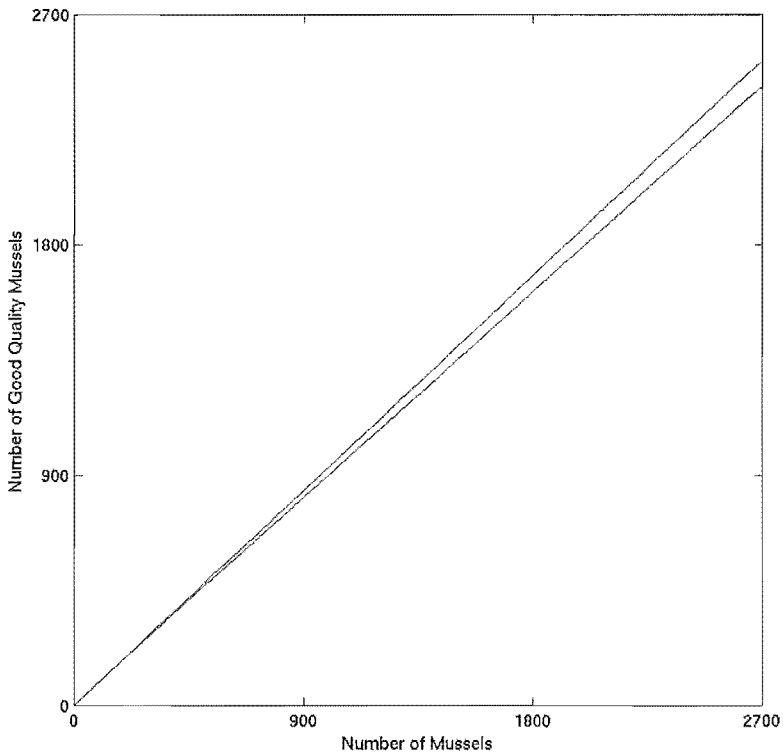

Figure 18. Efficiency of rows of units in unidirectional flow. The upper curve is for a row perpendicular to the flow and the lower curve is for a row parallel to the flow.

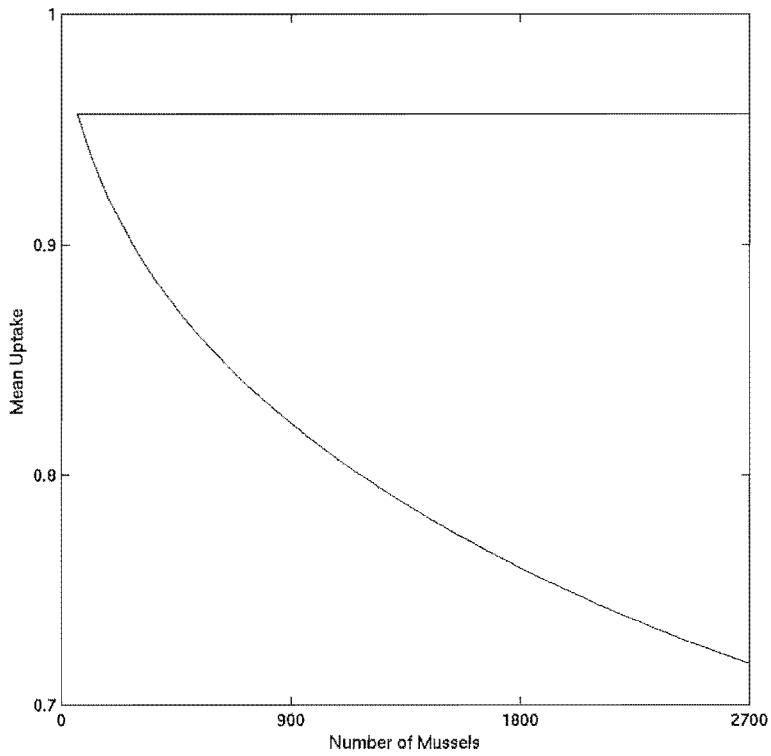

Figure 19. Efficiency of sheets of units in unidirectional flow. The upper curve is for a sheet perpendicular to the flow and the lower curve is for a sheet parallel to the flow.

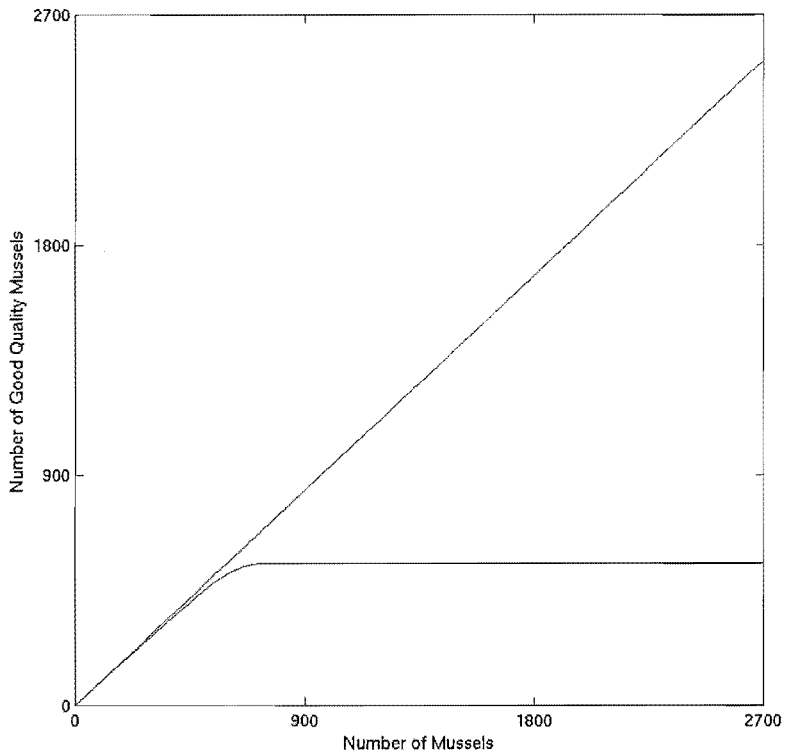

Figure 20. Efficiency of sheets of units in unidirectional flow. The upper curve is for a sheet perpendicular to the flow and the lower curve is for a sheet parallel to the flow.

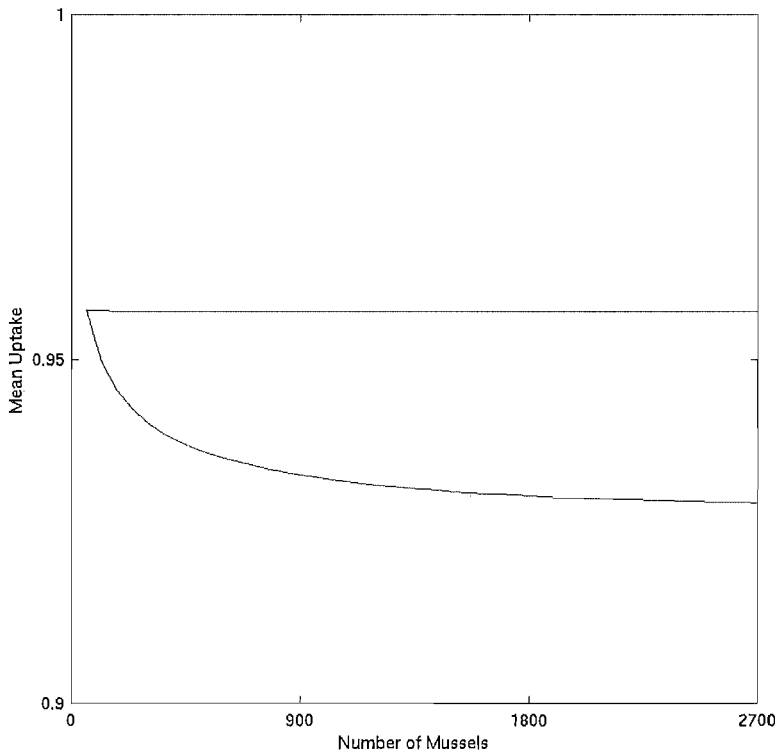

Figure 21. Efficiency of rows of units in varied flow. The upper curve is for a vertical row and the lower curve is for a horizontal row.

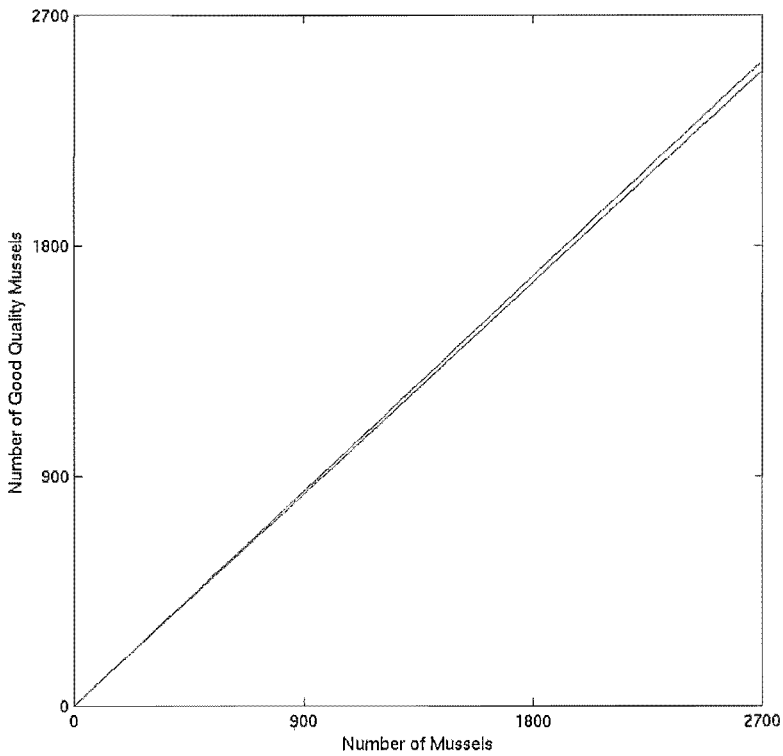

Figure 22. Efficiency of rows of units in varied flow. The upper curve is for a vertical row and the lower curve is for a horizontal row.

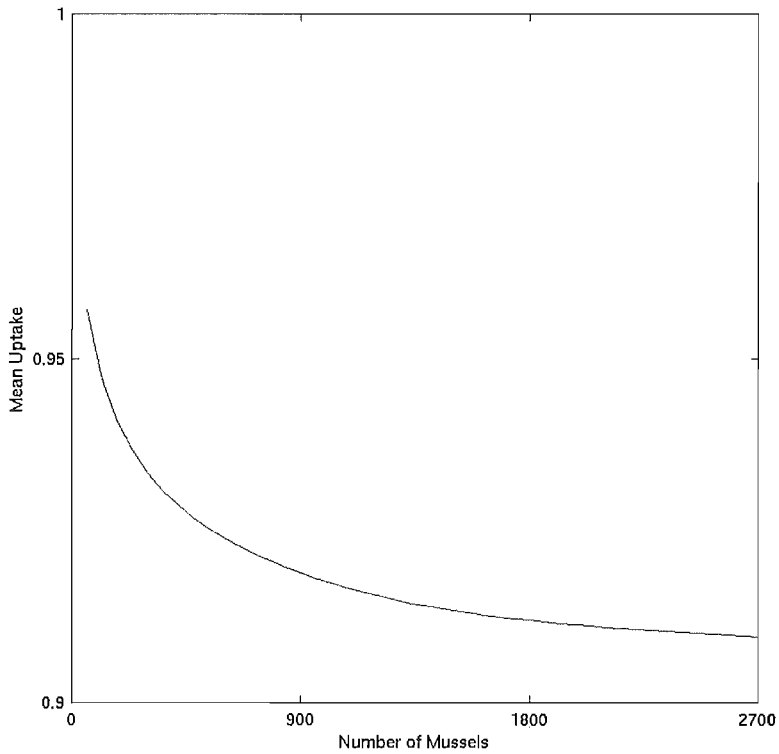

Figure 23. Efficiency of a vertical sheet of units in varied flow.

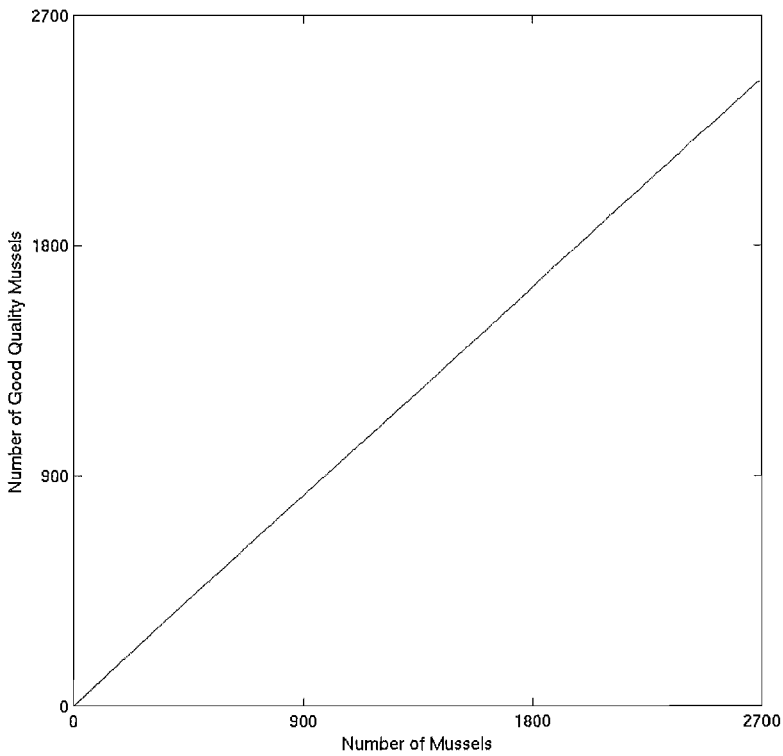

Figure 24. Efficiency of a vertical sheet of units in varied flow.

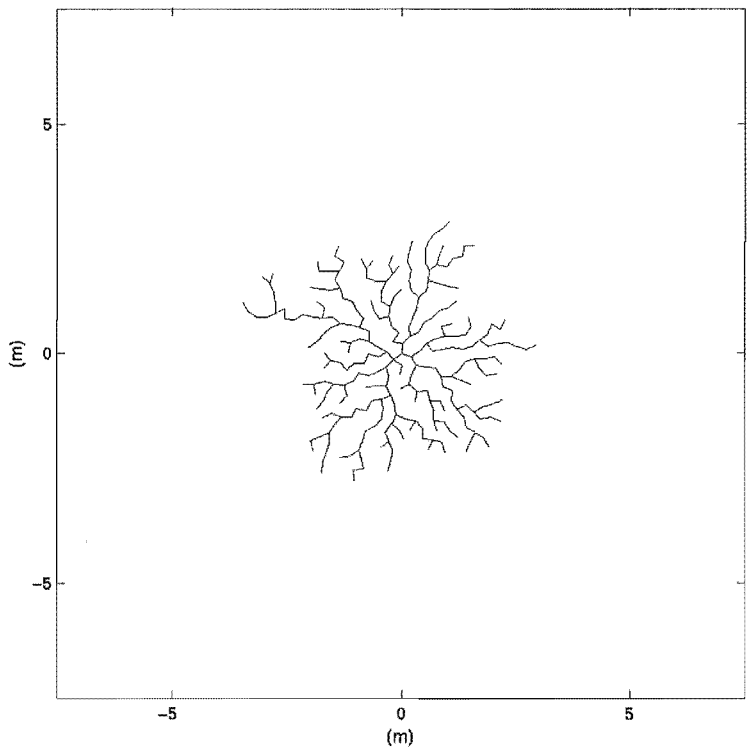

Figure 25. Two dimensional branching structure, generated with no optimality consideration of flow condition. 270 units of mussels in total.

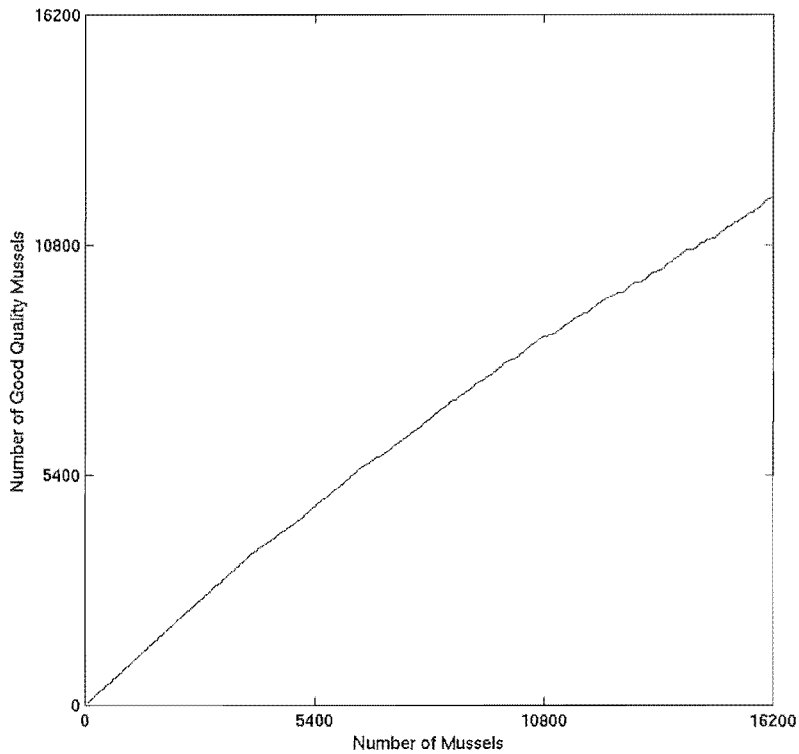

Figure 26. Progressive efficiency of branching structure during growth.

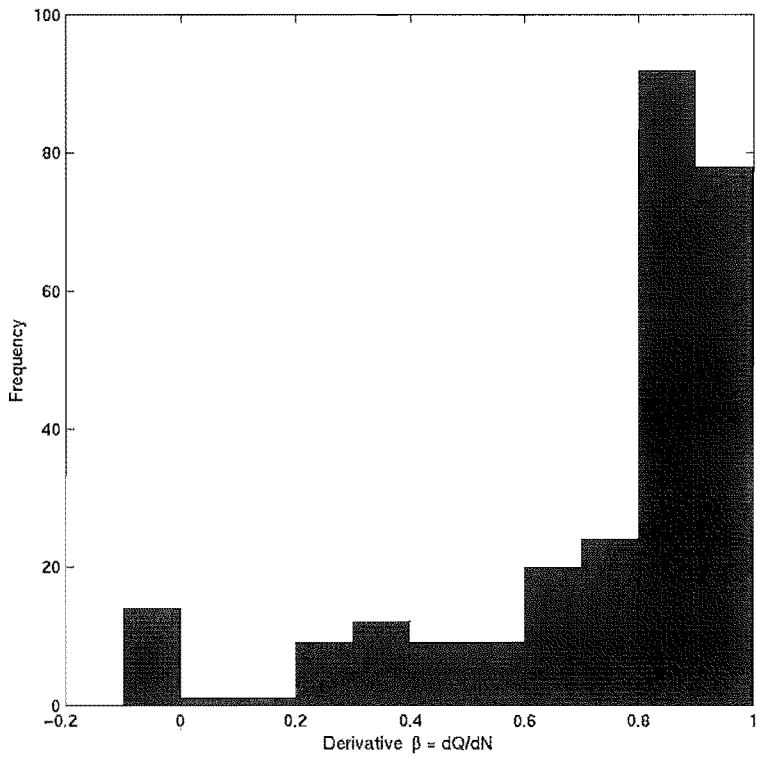

Figure 27. Distribution of the derivative of the efficiency progression curve for the branching structure.

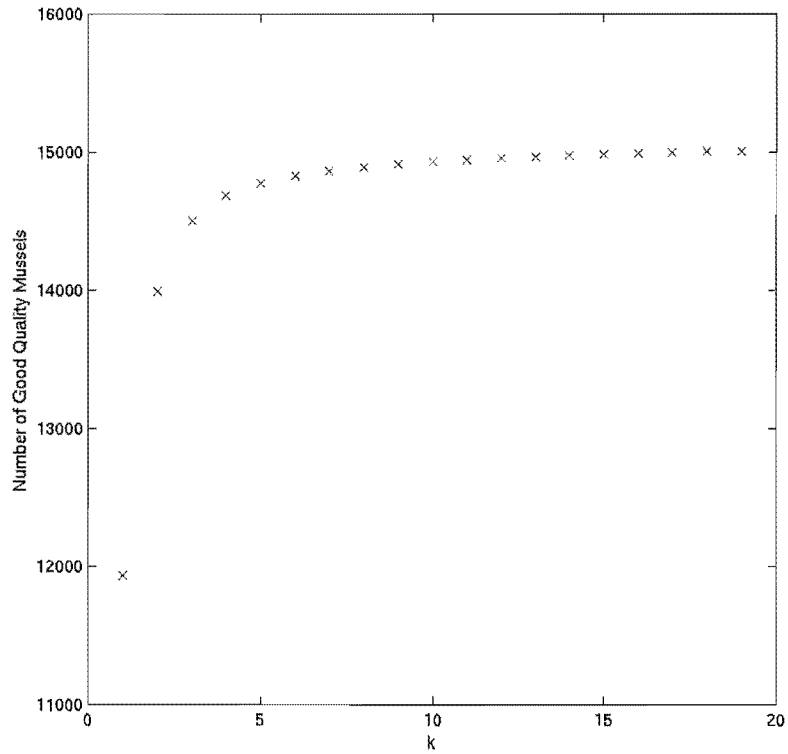

Figure 28. Projected efficiency for various k, the number of possibilities for iterative extension for the branching structure.

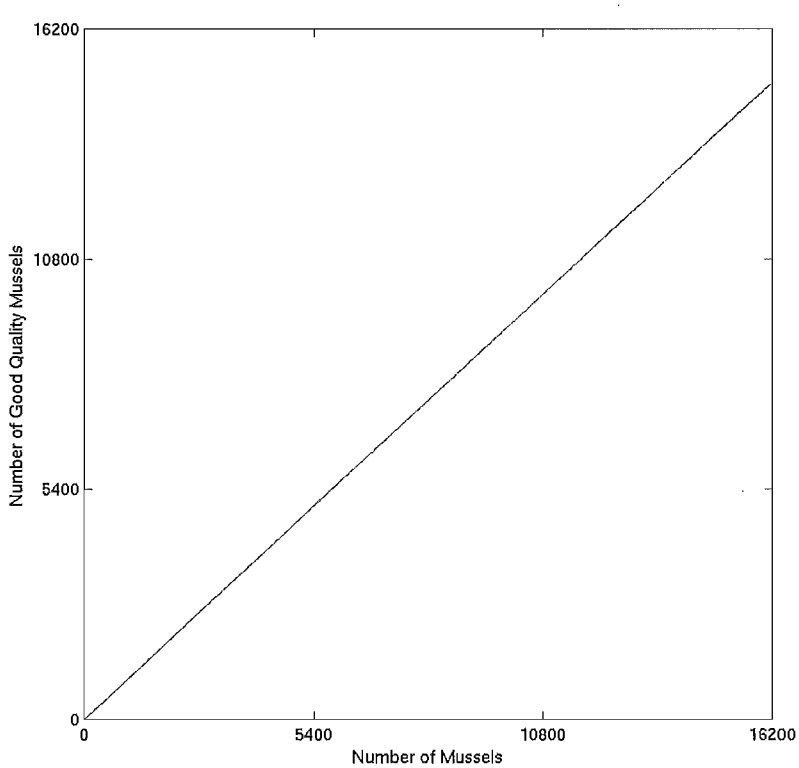

Figure 29. Projected efficiency curve for $k = 10$, compared with results from simulations. The two curves are indistinguishable.

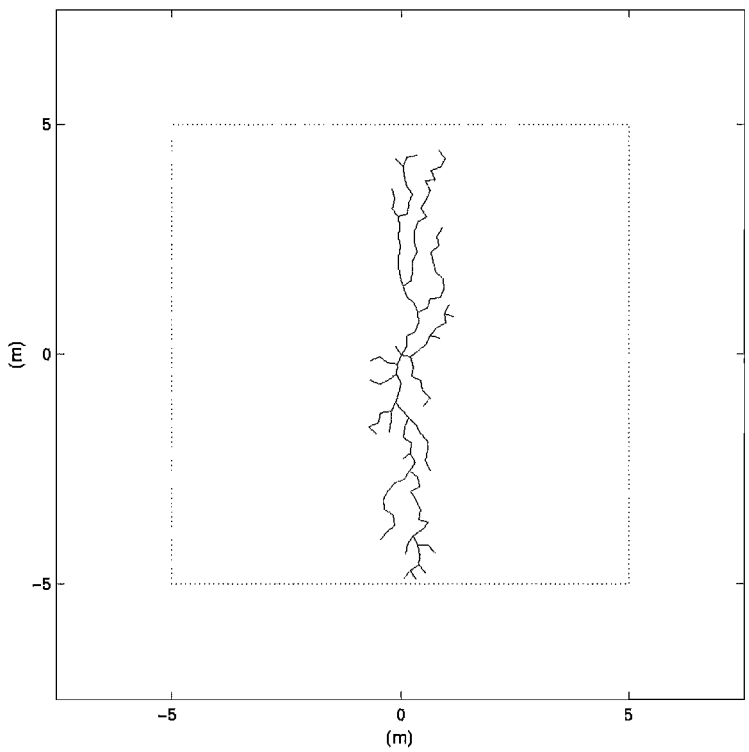

Figure 30. Branching structure for unidirectional flow, with 10 m spatial limit, after 135 units. Flow is from left to right.

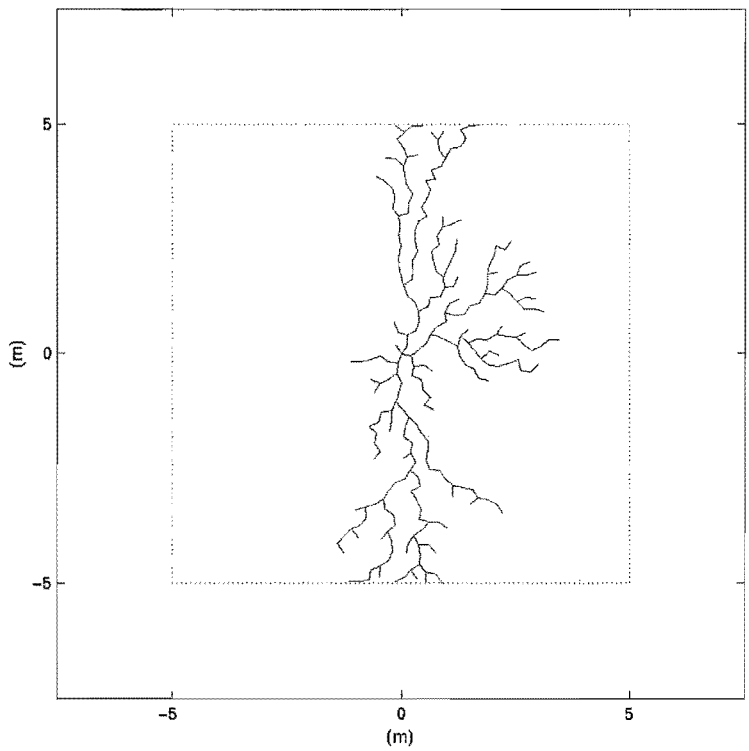

Figure 31. Branching structure for unidirectional flow, with 10 m spatial limit, after 270 units. Flow is from left to right

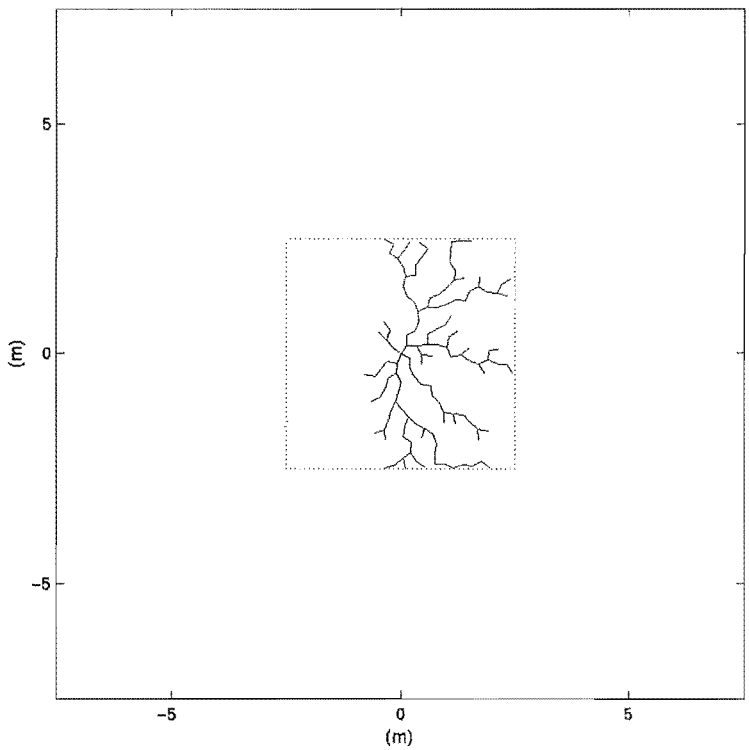

Figure 32. Branching structure for unidirectional flow, with 5 m spatial limit, after 135 units. Flow is from left to right.

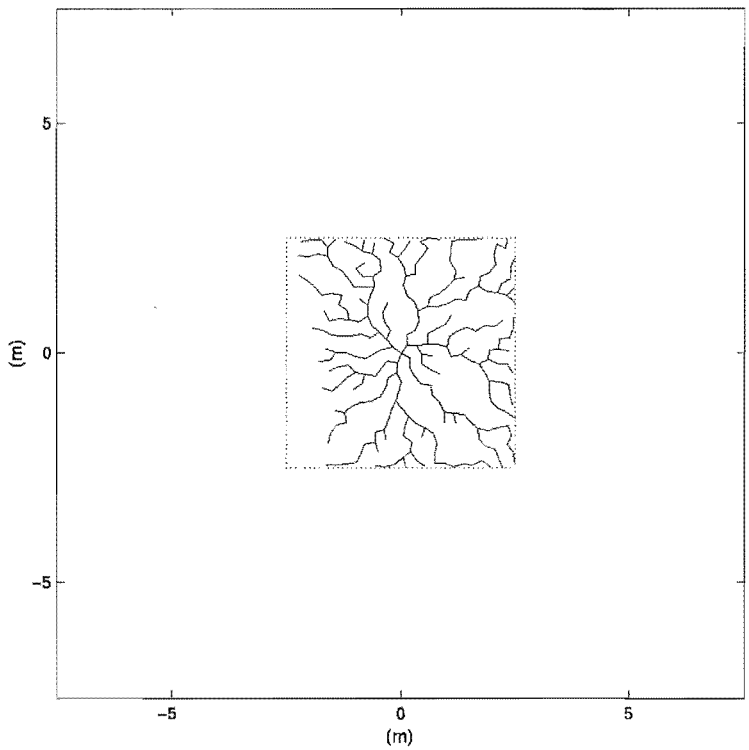

Figure 33. Branching structure for unidirectional flow, with 5 m spatial limit, after 270 units. Flow is from left to right.

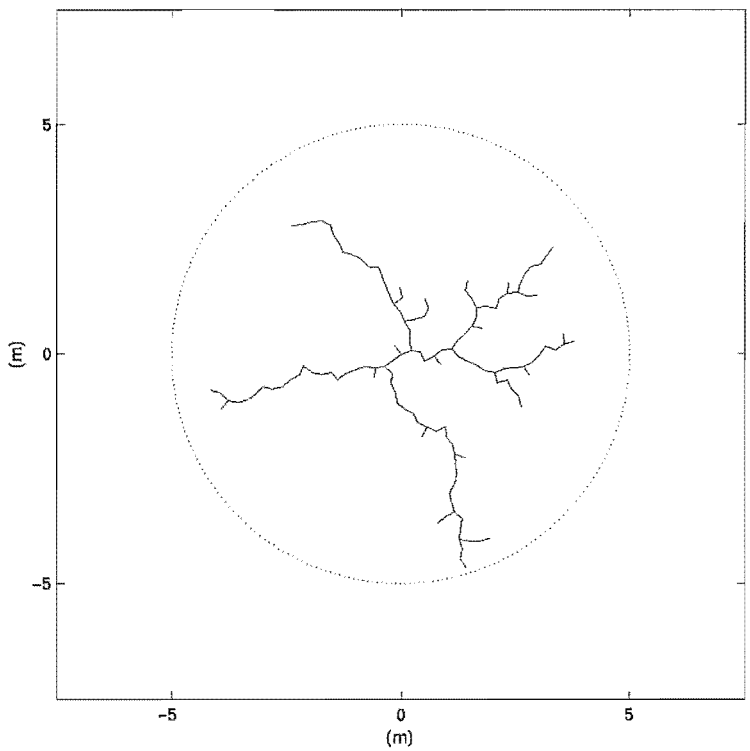

Figure 34. Branching structure for varied flow, with 10 m spatial limit, after 135 units.

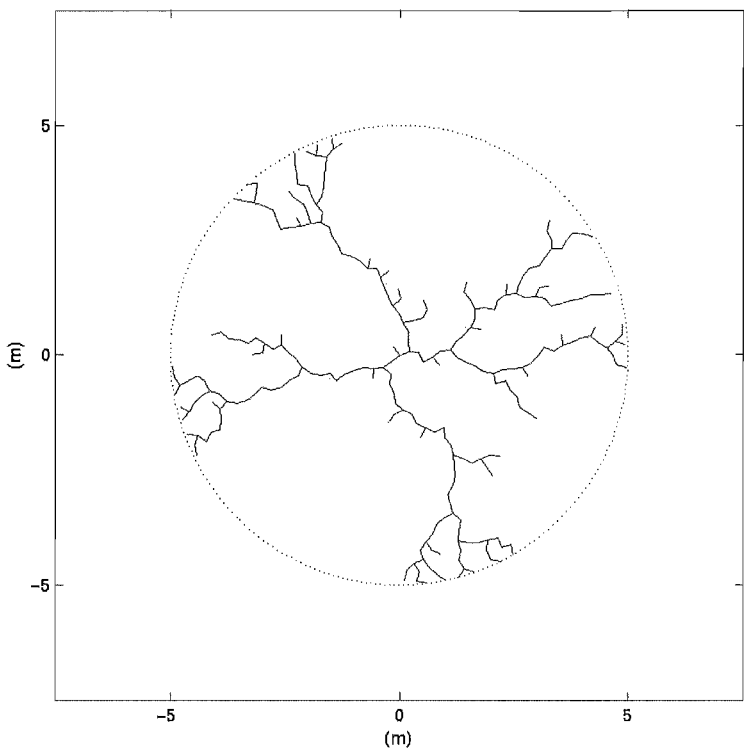

Figure 35. Branching structure for varied flow, with 10 m spatial limit, after 270 units.

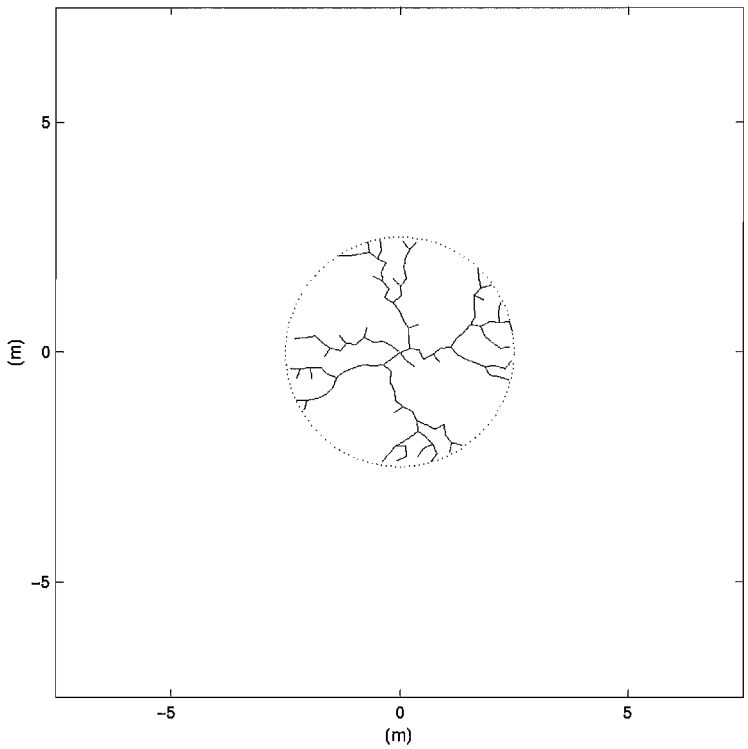

Figure 36. Branching structure for varied flow, with 5 m spatial limit, after 135 units.

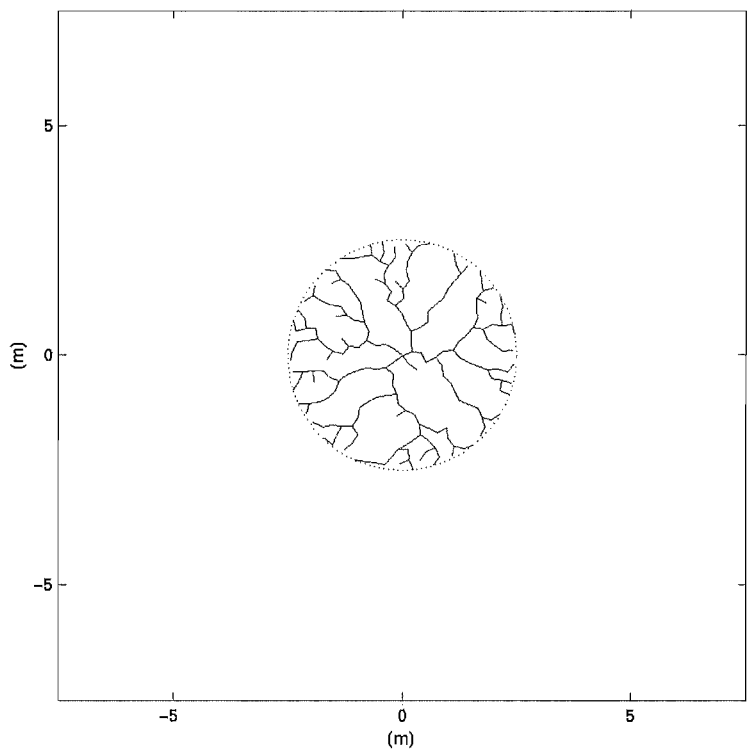

Figure 37. Branching structure for varied flow, with 5 m spatial limit, after 270 units.

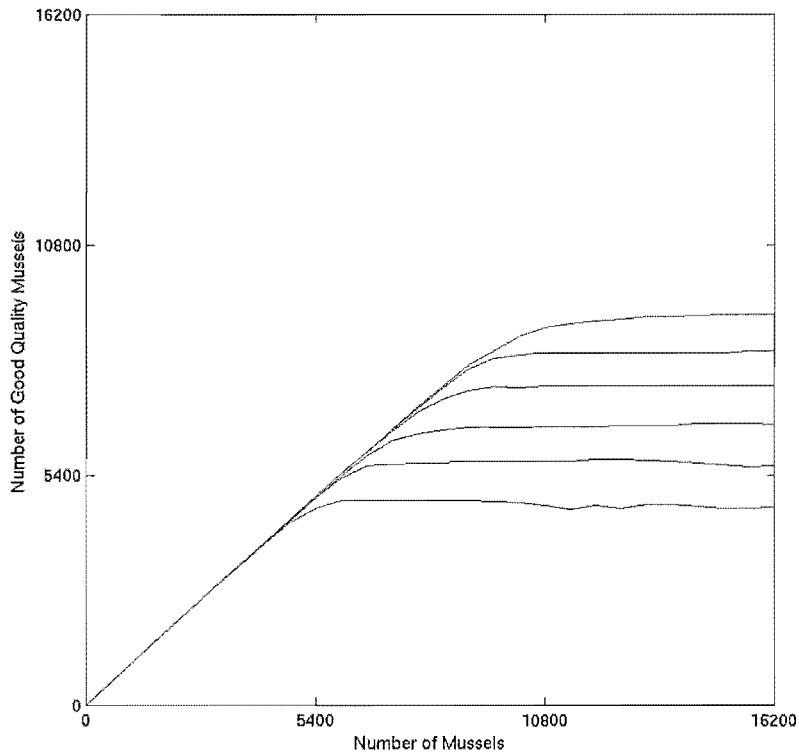

Figure 38. Efficiency for branching structures in unidirectional flow, with various spatial limits. The lowest curve represents the 5 m case, progressing up to the highest curve for the 10 m case.

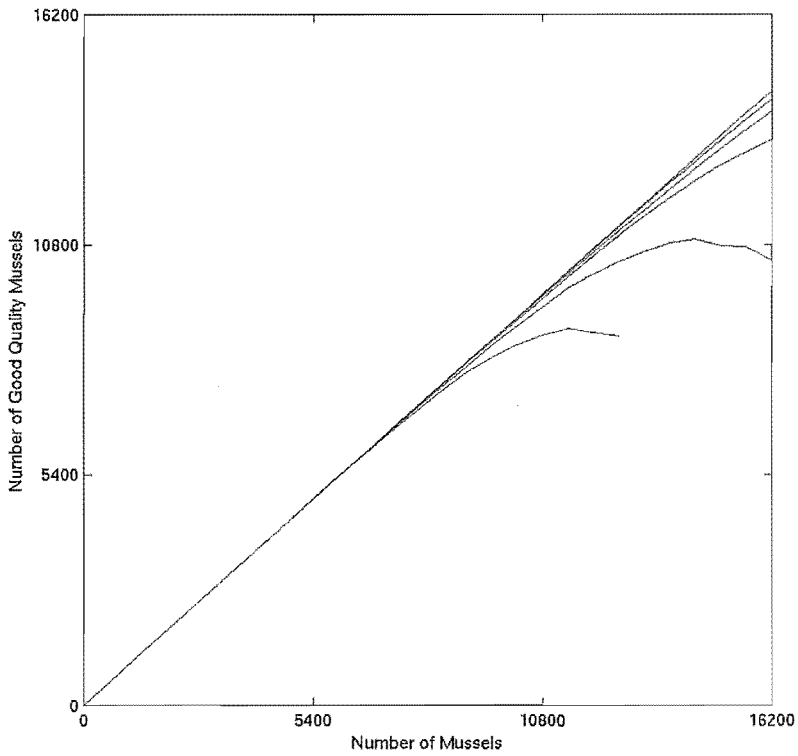

Figure 39. Efficiency for branching structures in varied flow, with various spatial limits. The lowest curve represents the 5 m case, progressing up to the highest curve for the 10 m case.

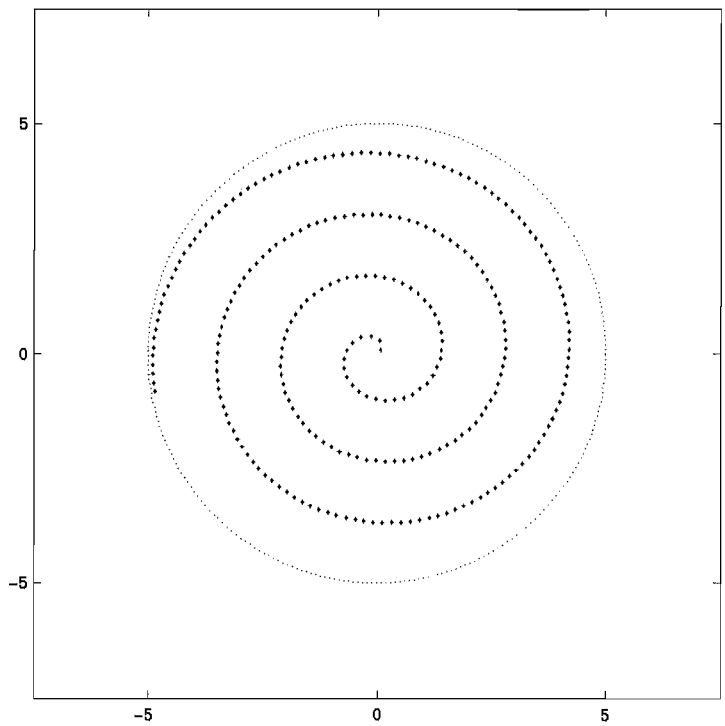

Figure 40. Designed structure for varied flow, with 10 m spatial limit and 270 units.

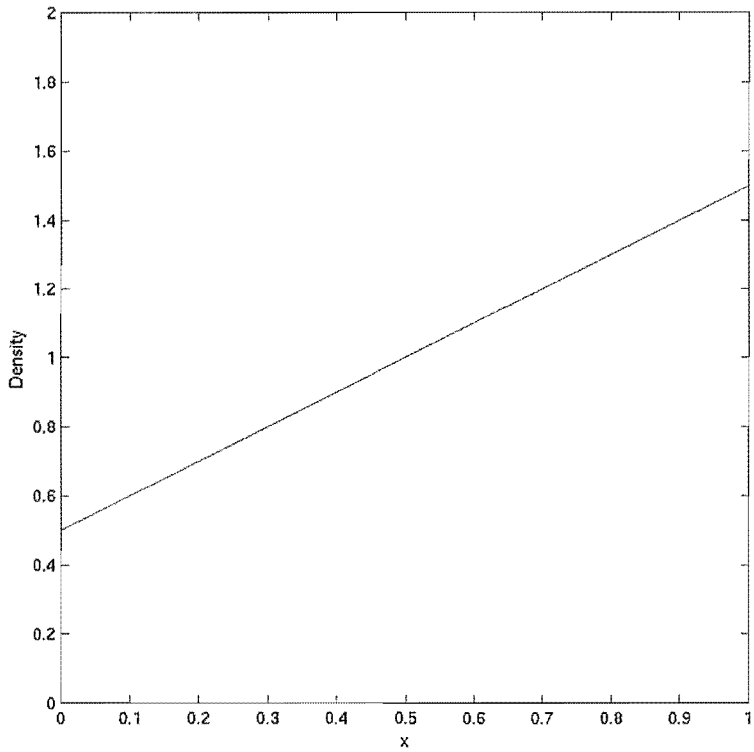

Figure 41. Spatial gradient of density of unconnected units of mussels. Here, $s = 0.5$. The x axis is parallel to the flow.

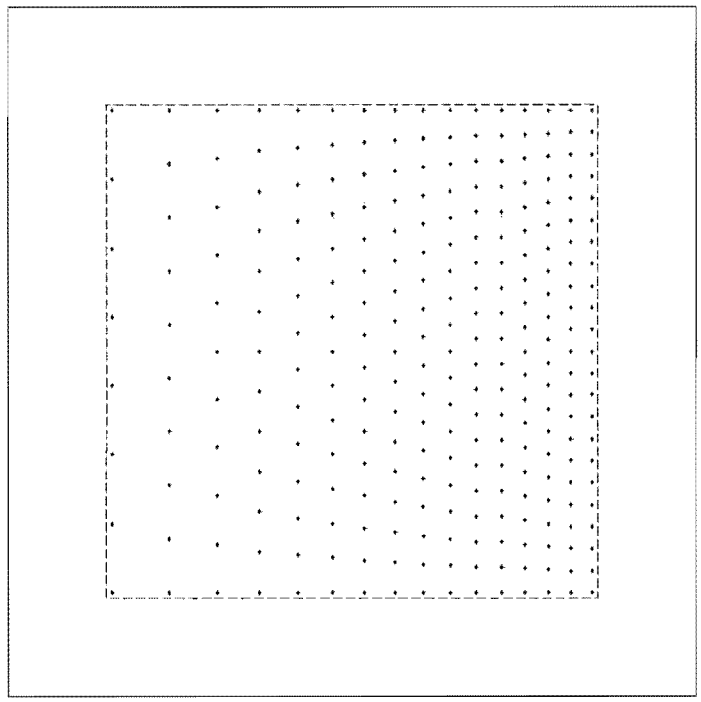

Figure 42. Example layout for an unconnected structure, with s = 0.5. Flow is from left to right. Units here are dimensionless, but the layout will be scaled to 10 m across.

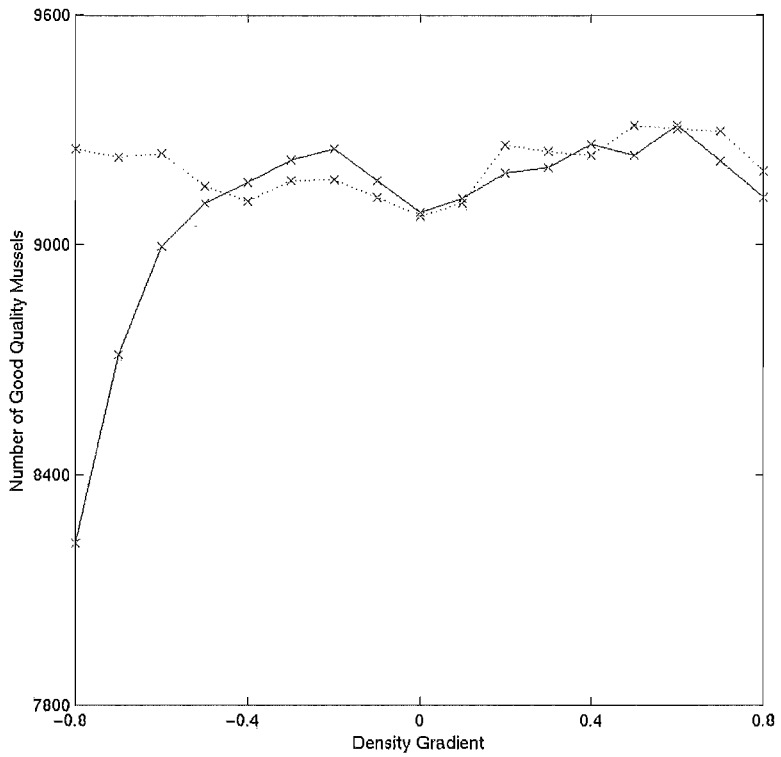

Figure 43. Efficiency for unconnected arrangements in unidirectional flow, with varying density gradients. The dotted line represents gradient varying with x (parallel to the flow) and the solid line represents the gradient varying with $|x|$.

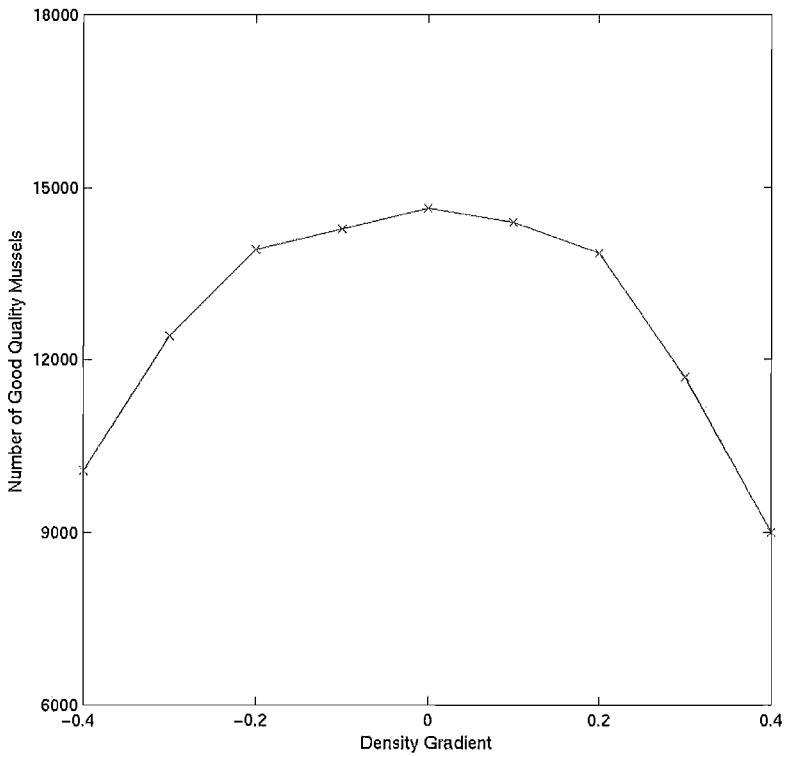

Figure 44. Efficiency for unconnected arrangements in varied flow, with density gradient varying with x (parallel to the flow).

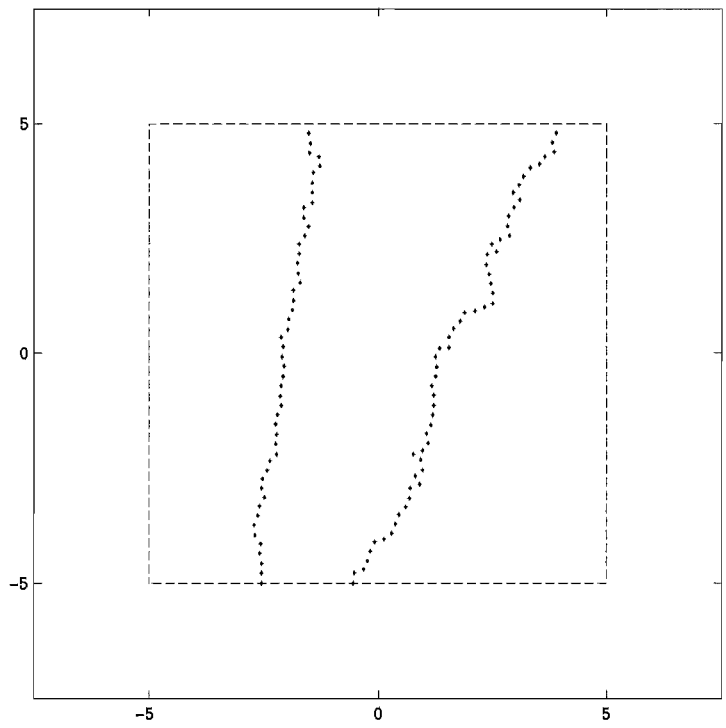

Figure 45. Chain structures after perturbation algorithm for optimisation. Flow is unidirectional, from left to right. The left and right hand structures are of 50 and 60 units respectively.

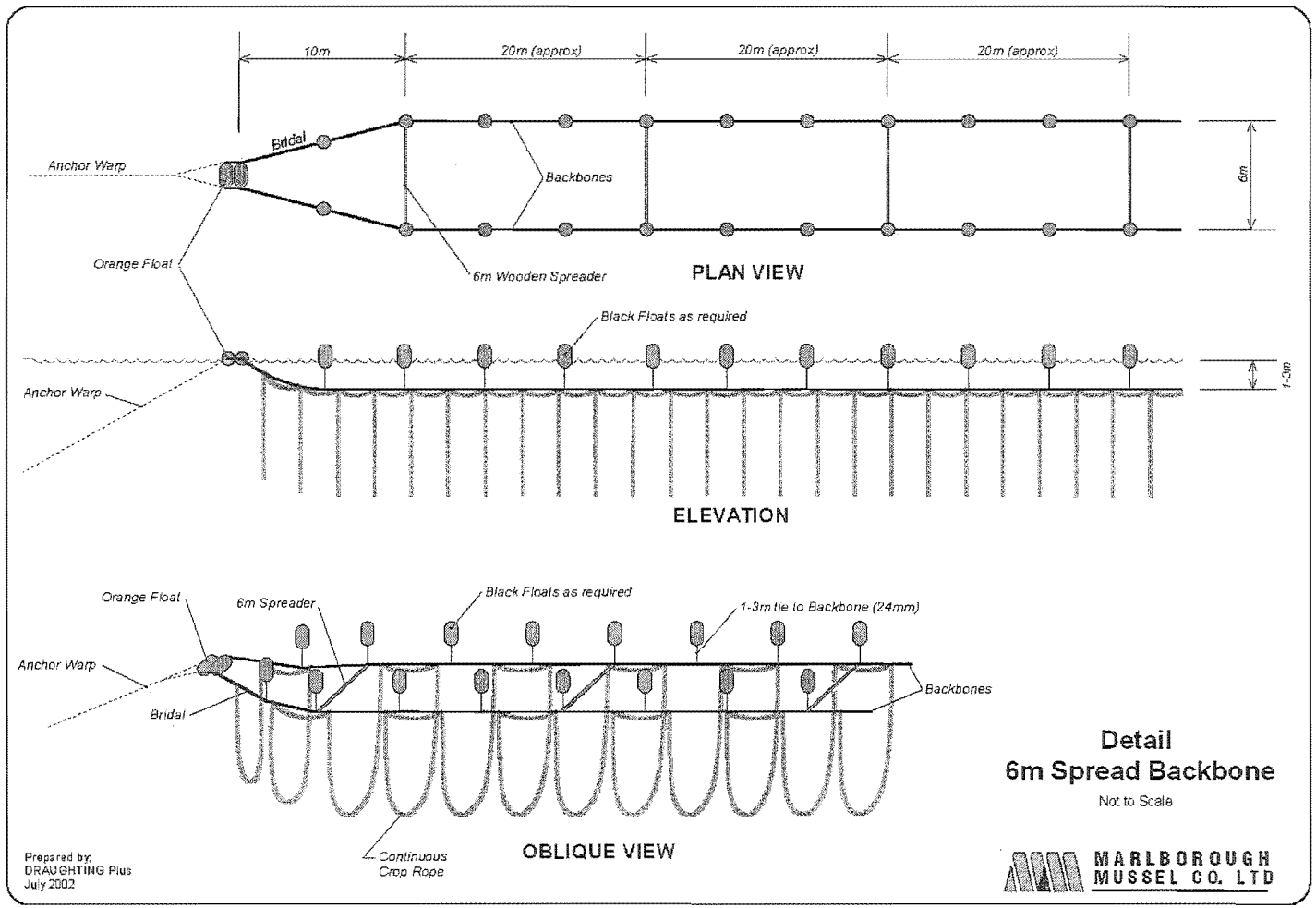

Figure 46. An example of one arrangement of mussels on an existing mussel farm.

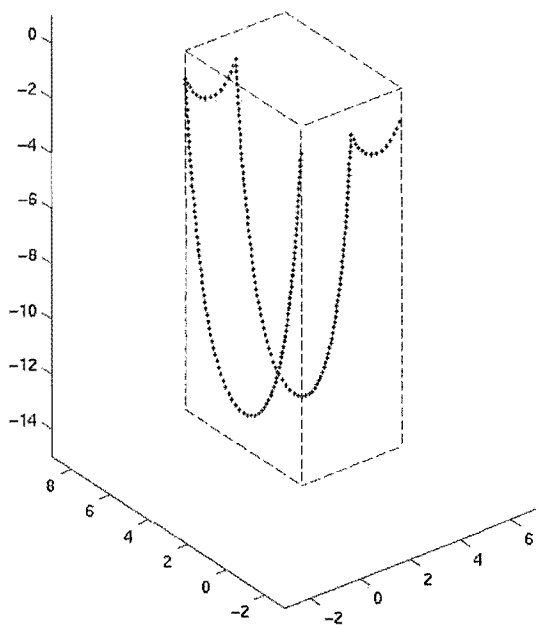

Figure 47. Computational model of existing arrangements.
All dimensions are represented here in metres.

Appendix A – LATTICE GAS AUTOMATA

During early stages of research, a Lattice Gas Automaton (LGA) model was developed as a potential simulation environment for hydrodynamics. Some of this research has been applicable to the Lattice Boltzmann method, the model employed for documented simulations. Some of the LGA issues will be detailed here, first relating to the structure of the model, then consideration of fluid incompressibility. Lastly, difficulties found in this approach will be discussed, primarily in relation to a drag coefficient experiment.

A Lattice Gas Automaton consists of a hexagonal grid structure in two dimensions. The basis for employing a hexagonal structure is its inherent symmetry, which ensures isotropic fluid behaviour (See Section 3.4 for further discussion on isotropy). Each cell represents a quantity of fluid, containing up to six particles of equal mass, potentially one for each lattice direction. Since there are six directions of the lattice, maintaining a mean of three particles per cell provides distributional symmetry and also maximum potential range of cell momentum. Particles move into adjacent cells according to their associated velocities. The update rule incorporates three particle processes. After the movement from cell to cell, particles collide and are reoriented. Lastly, particles reflect off preset boundaries or obstacles.

When particles collide, they are assigned a new velocity in such a way as to conserve physical quantities such as mass and momentum of the fluid in the cell. The combination of velocities in each cell is mapped by an operator to another combination. Of the sixty-four possible combinations, twenty of these undergo transformations, specified individually by way of a lookup table.

An overall fluid velocity is implemented on the system by forcing an excess of particles of a certain direction somewhere on the grid, for example on the left hand edge. Local fluid velocity at a point on the grid is then obtained by measuring the proportion of

particle types in its' neighbourhood, for example, the difference between right and left going particles within a given radius of the cell. Equilibrium is attained when spatial or temporal velocity averages approach stable values.

One of the key properties of water is its incompressibility, so it is vital that this model reproduces this property. Empirical measurements of fluid density are taken over spatial regions at a much larger scale than that of the fluid particles, that is, water the molecules. In a lattice system, however, there is not the luxury of spanning such large regions, since densities are required over areas comparable with only a few cells. Some statistical fluctuation would naturally be expected in cell density, which would not be attributed to fluid compression within the model. A useful measure is needed, to quantify this fluctuation and therefore produce an objective assessment of compressibility.

Let $p(i)$ be the probability distribution defined by $p(i)$ = the proportion of grid cells with i particles, i taking values 0 to 6. Initially the fluid field is constructed randomly. In each cell, the presence of a particle in each direction is independently random, each with probability 0.5. Thus the distribution $p(i)$ before any iterations is equivalent to a binomial distribution with 6 trials and probability 0.5. If $p(i)$ after several iterations is a 'flatter' distribution than binomial, there are disproportionate quantities of high and low density. It follows therefore that the standard deviation σ of $p(i)$ will be a direct measure of compressibility, the datum for comparison being that of the binomial distribution, namely $\sigma_B = \sqrt{6}/2 = 1.22$.

Experiments monitoring σ with time were performed for scenarios of no flow and for high velocity in which total momentum, oriented in the 'x' direction, was twice the momentum oriented in the '$-x$' direction. Arbitrary solid boundaries were also placed in the interior of the modelling domain to produce a non-uniform flow field.

Results showed that this value of 1.22 was maintained for simulations with zero velocity, but that increased flow generated regions of high and low density, causing σ to increase to a maximum of approximately 1.6. This represents a significant weakness in the model.

To further gauge the effect of high velocity on the behaviour of the model, simulations were conducted for flow past a cylinder, at Reynolds numbers ranging over approximately two orders of magnitude. This range was attained by varying both fluid velocity and cylinder diameter. For each simulation, the force on the cylinder was calculated by summation of the x component of the particle reflections in each time iteration. The drag coefficient was directly deduced from the force (See Section 3.5 for the same experiment using the Lattice Boltzmann model).

The computational experiment was designed such that certain Reynolds number values were generated with many combinations of velocity and diameter. Ideally, drag coefficient for a cylinder is dependent on the Reynolds number only, so that these combinations should produce the same result. Results were such that the multiple curves of drag coefficient against Reynolds number did not collapse onto the same values.

This result and the aforementioned indications of compressibility, are major problems for the LGA model, which could not be satisfactorily resolved. This modelling approach was therefore abandoned. It is noted that LGA have been used successfully by others (See references in Section 3.2), even though it is known that lattice gas models are unable to reach high grid-scale Reynolds numbers. These tests may be exposing problems in the implementation or coding of the model, rather than weaknesses in the model itself.

Appendix B – COMPUTER MODELLING OF AVALANCHE DYNAMICS AND TOPOGRAPHY

As part of a project entitled "Granular Avalanches and Surface Geometry: Physical Experiments and Computer Simulations" (Nikora V., Smith A., Walsh J., Image K., Gunn D. Eos Trans. AGU, 83(22) West. Pac. Geophys. Meet. Suppl., Abstract SE52D-10, 2002), a computer model of granular avalanching has been developed. This was carried out during the period of study documented in this thesis.

The objectives of the overall project were to test whether granular piles exhibit the behaviour of self-organised criticality and to identify any correlation between the avalanche dynamics and the geometry of the granular surface.

The two-dimensional computer model was based on a simple model of sandpile generation, whereby an active particle rolls down the surface of the pile in the direction of its steepest angle of descent, until settlement at a local minimum in surface elevation. This surface generation model does not address avalanche dynamics, since settled particles become permanently inactive. Simulations were performed with circular particles whose diameter followed a log-Normal distribution.

This basic model was developed to simulate avalanching by imposing a critical local surface angle. A static particle was activated if its angle was above the threshold and if contacted by an active particle. Settlement thereafter, of both particles, followed the path of steepest descent.

Further, a third model was designed, which incorporated inertial forces between particles. Activation of a static particle would occur if its angle was above the threshold and if contacted by an active particle of greater mass.